Experimental Evaluation of an Additively Manufactured Straight Mini-Channel Heat Sink for Electronics Cooling

Ali F. Eidi

Thesis submitted to the Faculty of the
Virginia Polytechnic Institute and State University
in partial fulfillment of the requirements for the degree of

Master of Science
in
Mechanical Engineering

Scott T. Huxtable, Chair
Thomas E. Diller
Christopher B. Williams

Feb. 19 2021
Blacksburg, Virginia

Keywords: Heat Transfer, Additive Manufacturing, Binder Jetting,
Minichannels/Microchannels, Heat Sinks, Electronics Cooling

Experimental Evaluation of an Additively Manufactured Straight Mini-Channel Heat Sink for Electronics Cooling

Ali F. Eidi

(ABSTRACT)

The continuous miniaturization of electronic devices and the corresponding increase in computing powers have led to a significant growth in the density of heat dissipation within these devices. This increase in heat generation has challenged conventional air fan cooling and alternative solutions for heat removal are required to avoid overheating and part damage. Micro/Mini channel heat sinks (M/MCHS) that use liquids for heat removal appear as an attractive solution to this problem as they provide large heat transfer area per volume. Mini/microchannels traditionally have suffered from geometrical and material restrictions due to fabrication constraints. An emerging new additive manufacturing technique called binder jetting has the potential to overcome some of those restrictions. In this study, a straight minichannel heat sink is manufactured from stainless steel using binder jetting, and it is experimentally evaluated. The hydraulic performance of the heat sink is tested over a range of Reynolds numbers (150-1200). The comparison between the hydraulic results and standard correlations confirms that the targeted geometry was produced, although the high surface roughness created an early transition from laminar-to-turbulent flow. The heat transfer performance was also experimentally characterized at different heat flux conditions ($3000 W/m^2$, $5000 W/m^2$, $6500 W/m^2$), and a range of Reynolds numbers (150-800). These results indicated that convection heat transfer coefficients on the order of $1000 W/m^2 - K$ can be obtained with a simple heat sink design. Finally, the effects of the contact resistance

on the results are studied, and contact resistance is shown to have critical importance on the thermal measurements.

Experimental Evaluation of an Additively Manufactured Straight Mini-Channel Heat Sink for Electronics Cooling

Ali F. Eidi

(GENERAL AUDIENCE ABSTRACT)

The field of electronics is experiencing two phenomena that are causing significant increase in the heat generated in modern devices. One is that the electronic devices are getting smaller, and second, the density of the processors (the component responsible for executing instructions) is increasing. Those two characteristics have increased the amount of heat generated, and it is becoming increasingly difficult to remove that heat using a typical classical air fan cooling system seen in a common computer. Therefore, creative designs and solutions are required in order to remove that heat and keep the processor temperature low to avoid part damage or failure. One solution that is attractive is the use of micro/mini channel heat sinks (M/MCHS) with water cooling instead of air. A micro/mini channel heat sink is a device that is used to transfer heat from a processor to a fluid to regulate the temperature. Micro/mini channel heat sinks have extremely small fluid channels fabricated on the surface, and they have several features that make them suitable for cooling electronic devices. Those characteristics include: high surface-to-volume ratio, low weight, and high heat transfer coefficient (where the heat transfer coefficient characterizes how easily heat is removed from a surface). However, one drawback of these heat sinks is that the small fluid channel sizes make them very difficult to manufacture. If one aims to create interesting designs for the channels, such as incorporating curved surfaces, it becomes excessively difficult or even impossible to fabricate these shapes using traditional manufacturing methods. One way to overcome those design restrictions is to used additive manufacturing (i.e. three dimensional,

or 3D, printing). A process called binder jetting is one type of 3D printing that processes unique advantageous. Binder jetting involves the use of a precisely controlled printer for the application of liquid glue (binder) on a fine powder bed to bind powder create the exact shape that is desired. The advantages of binder jetting include that it is low cost, high speed, that it can be applied to a variety of materials, and the ability to scale the process easily in size. In this study, a straight minichannel heat sink manufactured using binder jetting with stainless steel is experimentally evaluated. The heat sink was evaluated, for both its fluid flow (hydraulic) and thermal characteristics. The hydraulic evaluation is a study of the pressure drop (the difference in pressure between the beginning and the end of the heat sink) and the friction of the fluid flowing through the channel. To evaluate the pressure drop, the flow rate (the volume of liquid passing through the heat sink per unit of time) of the liquid through the channels is varied from 2 to 20 gallons per hour (corresponding to Reynolds numbers of 150-1200), during which the pressure drop data is recorded. After the experiment is finished, the data are compared to an established correlation (a statistical relationship between friction factor and Reynolds number). This comparison showed two important findings. One is that there is an agreement between the experimental results and the correlation, which indicates that binder jetting was able to accurately produce the part with specified design dimensions. Another important finding is that the flow exhibits an early transition from laminar-to-turbulent flow. The transition from laminar flow (smooth flow with little mixing) to turbulent flow (chaotic flow) usually occurs at around a Reynolds number of about 2300. However, the 3D printed sample experienced this transition at a Reynolds number of about 500. Parts made with additive manufacturing have an inherently high surface roughness, which is believed to be the reason behind this early transition to turbulence. The effect of the roughness on the flow should be carefully considered in future designs of 3D printed minichannels. The other part of the evaluation is the thermal performance of the heat sink. For the thermal performance, heat is supplied to

the samples, and the value of the heat transfer coefficient is measured at different flow rates. The results show that a high value of the heat transfer coefficient can be achieved with a simple design for the additively manufactured heat sinks.

Acknowledgments

I would like to express my sincerest gratitude for my advisor Dr. Scott Huxtable for granting me the opportunity of working under his supervision. Dr. Huxtable has been a source of insightful and creative ideas throughout my studies. His philosophy of providing feedback without imposing provided an environment of freedom to perform and enjoy my own thesis. Dr. Huxtable has also worked very closely with me, by having late and frequent meetings, to meet deadlines and achieve good results. In addition of guiding me to achieve my academic goals, Dr. Huxtable also helped shaped my overall personal character. I thank him very much.

I would like to also thank my committee members, Dr. Diller and Dr. Williams for their continuous guidance during the project.

I would also like to thank my lab colleagues: Dr. Ali Roghanizad, and Mohammed AlEnezi for their input and help in the heat transfer part of the study.

Our friends at the DREAMS lab, Kazi Rahman and Danny Rau, provided constant support on the 3D printing side of the project. I am very thankful for their help.

I am truly thankful to all my family members, especially my father. Last summer, during the peak months of quarantine and isolation, I worked closely with my father, Mr. Fadhil Eidi, to design the sample holder in the experiment. Even though he does not come from an academic background, he did provide creative insights on the design of the holder, methods to fabricate the holder, and ways to seal water leaks. His effort in this project reminded me of when he was helping me with a school project about birds in the 3rd grade. The two projects are 17 years apart but he showed the same level of enthusiasm and love. He has always been a source of support and encouragement in every step of my life. Therefore, I

would like to thank him for his role in this thesis, the bird project, and all the sacrifices in between.

I would like to also thank my friends here in Blacksburg and back in Kuwait.

Finally I would like to thank Dr. Stephen R. Covey. His teachings have shaped the way that I see life. Also, his books played an important part in finishing this thesis, because I used them as a guide and a reference during difficult times.

Contents

List of Figures

List of Tables

Chapter 1

Introduction

The continuous miniaturization of electronic devices and the corresponding increase in computing powers have led to a significant growth in the density of heat dissipation within these devices [1]. This increase in heat generation has challenged conventional air fan cooling and alternative solutions for heat removal are required to avoid overheating and damage to the devices. A report from the International Technology Roadmap for Semiconductors [2] states that heat fluxes of about $100 W/cm^2$ are to be removed from electronic chips, and between 100-300 W/cm^2 for laser diodes [3], which reaches the limit of conventionally air cooled fan-assisted heat sinks [4]. Additionally, Krishnan et al. [5] predict that in the near future, the demand of cooling for electronic devices is to reach $1000 W/cm^2$.

Micro/Mini channel heat sinks (M/MCHS) that use liquids for heat removal emerge as an attractive solution to the problem of high heat flux as they provide large heat transfer area per volume [6]. Microchannels are capable of removing up to $1000 W/cm^2$ [7], whereas conventional channel heat sinks dissipate up to $20 W/cm^2$ [8]. Microchannels are one of the results of the miniaturization movement, and they have emerged as a vital option to find solutions to energy management issues. There are a number of different definitions for microchannels that are used in literature, however, all of the definitions distinguish between mini, micro, and conventional channels using the hydraulic diameters (D_h) [1]. The classification presented by Kandlikar and Grande [9] (shown in Table 1.1) are the most popular in the literature.

Table 1.1: Nomenclature and classification used by Kandlikar and Grande

Conventional Channels	$D_h > 3mm$
Minichannels	$200\mu m < D_h \leq 3mm$
Microchannels	$10\mu m < D_h \leq 200\mu m$
Transitional channels	$0.1\mu m < D_h \leq 10\mu m$
Molecular nanochannels	$D_h \leq 0.1\mu m$

The cooling ability of M/MCHS is related to the high heat transfer coefficient which is gained by the small channel diameter and the large surface-to-volume ratio [10]. Nevertheless, those advantages come at a cost of high pressure drop and increased pumping power. Also, M/MCHS still face the problem of temperature variation in the flow direction due to the thickening of the boundary layer [10].

Numerous researchers have attempted to understand the hydro-thermal performance of M/MCHS and in the next subsection, the relevant literature is summarized to explain the current state of the art as well as the future potential of M/MCHS.

1.1 Literature Review

The concept of microchannel heat sinks (MCHS) first emerged in a famous paper by Tuckerman and Peace [11]. They were able to remove heat up to $800 W/cm^2$, and they mentioned that as the hydraulic diameter decreases, the heat transfer coefficient increases. Their paper was followed by another milestone paper by Philips [12] in which he analyzed carefully the heat transfer and provided equations and guidelines for the design of microchannel geometries. Kandlikar et al. [13] presented a procedure for selecting the microchannel geometry while trying to minimize pressure drop. They concluded that it is important to incorporate enhancement features and shorter lengths in the microchannel to provide desired heat transfer results. Pokharna et al. [14] examined the use of microchannel heat sinks in a computer,

and they discussed the cost issues associated with mass production of such systems.

The number of research papers related to microchannels have increased as the manufacturing techniques capable of producing them have gained popularity. Several review papers [15, 16, 17, 18, 19, 20] have summarized what has been done in microchannels for different geometries, coolants, and materials. This literature review focuses on the different geometries of microchannel heat sinks, and is divided into three sections:

- Review of Straight Flow Patterns
- Review of Non-Straight Flow Patterns
- Additive Manufacturing & Microchannels

1.1.1 Straight Channel Flow Patterns

The geometry pattern of a microchannel has a great effect in the amount of heat transfer and pressure drop associated with the microchannel. The straight channel pattern was the first to be investigated [11]. More recently Gunnasegaran et al. [21], numerically investigated the effect of changing the cross-sectional area of the straight channel MCHS. They studied three different shapes: rectangular, trapezoidal and triangular. They found that the rectangular shape had the best heat transfer performance, followed by the trapezoidal. Morini [22, 23] tested out the same geometries, however, he added a hexagonal shape. He states that, microchannels with a hydraulic diameter of 1mm and less, a disagreement in the results obtained in experimental and conventional theory might require a new modified understanding to account for the difference. Other studies [24, 25, 26], also carried out experimental and numerical calculations on straight microchannel heat sinks with different cross-sectional shapes. However, they found that there is no significant difference in the heat

transfer coefficient or the pressure drop if the hydraulic diameter is the same.

Nevertheless, Morini [23] states that there is a significant disagreement between the experimental results and the conventional theory, and also between two different experimental studies. He proposed various reasons to account for those differences, including compressibility effects, viscous dissipation effects, surface roughness, and experimental uncertainties.

This disagreement between the different papers have ignited a spark of interest in studying the effect of surface roughness on the performance of microchannels heat sinks. Hu et al. [27] developed a numerical model to simulate the roughness effects. They stated that roughness element size, height, spacing and the channel area showed a great effect on both the pressure drop and the velocity profile. Rawool et al. [28] also numerically investigated the effect of surface roughness on the flow in a microchannel. They found that as the height of the element increases, the friction factor also increases in a nonlinear manner. They also stated that the roughness element shape effects the friction factors, as rectangular and triangular shapes have higher friction factor. Lastly, they [28] concluded that the pressure drop decreased with an increase in the roughness pitch. After adjusting for the effects of roughness, later papers seem to agree with laminar flow theory.

Escher et al. [29] studied the flow in straight microchannel heat sink with nanofluids. They fabricated three channels and studied their thermal performance at different concentrations of nanofluids. They found that to estimate the heat transfer performance, correlations can be used. Escher et al. [29] also noted that the the thermal conductivity enhancement must be larger than the viscosity increase in order to achieve high heat transfer performance.

1.1.2 Non-Straight Flow Patterns & Channels with flow disruption

The main idea of a non-straight flow pattern is to cause disruption and mixing of the flow which can interrupt the boundary layer and achieve higher heat transfer. However, this disruption is usually accompanied by an increase in pressure drop. In this section, some relevant non-straight geometries are discussed.

Alnaema et al. [30] studied, numerically and experimentally, liquid flow in serpentine microchannel heat sinks. In total, they had four different heat sinks, where the first one was a straight microchannel while the others had single, double and triple serpentine paths. Their [30] numerical results agree with the experimental studies and show that the single path serpentine heat sink had a higher average Nusselt number, by 35%, and lower thermal resistance (by 20%). They state that this high heat transfer is gained at the expense of an increase in pressure drop, and better design optimization should be aimed at reducing this penalty. Sui et al. [31] numerically investigated a different type of geometry, wavy microchannels. They found that vortices generated along the flow channel were chaotic and enhanced the fluid mixing which increased the heat transfer coefficient. Comparing the straight microchannels with wavy microchannels, the wavy microchannels had better heat transfer performance at the same cross-section. However, the pressure drop was also greater for wavy microchannels. Following that work, they also did an experimental study which agreed with the numerical findings [32]. Mohammed et al. [33] also experimented with wavy microchannels. They examined five different wave amplitudes and [33] found that increasing the wavelength increases the heat transfer coefficient. However, exceeding 500 μm resulted in poor performance. Mohammed et al. [34] also performed another interesting study, as they compared wavy microchannel with curvy and zigzag microchannels. The zigzag pattern

had the best thermal performance transfer but the highest pressure drop, whereas the step microchannel had the lowest heat transfer performance. Comparing the step pattern with the straight channel pattern showed that the step pattern had superior performance [34]. Another interesting study, by Khoshvaght et al [35], studied the effect of adding different configuration of nooks to the zigzag patterns. The nooks had triangular, rectangular and circular shapes, and were compared to the regular zigzag shape. The result of their study showed that the heat transfer performance was enhanced with adding nooks due to the swirl flow generated by the nooks [24]. Another type of geometry that has been studied extensively is the converging-diverging flow pattern. Duryodhan et al. [36, 37, 38] performed experimental and numerical studies of the flow in diverging and converging geometries and then they compared them to each other and to the straight flow pattern. The promising result that they found is that the converging pattern resulted in a significant enhancement of the heat transfer performance, and they concluded that a combined converging-diverging flow pattern is a worthwhile way to improve the heat transfer.

Interrupting the flow by using fins, ribs and dimples has great potential of increasing the heat transfer rate while maintaining a low pressure drop [39]. Interruptions, like pin fins, not only increase the surface area but also generate better flow mixing, which enhances the heat transfer [40]. Wei et al. [41] and Xu et al. [42] studied rectangular microchannels with internal shapes along the bottom surface of the channel. Both papers shows an increase in the Nusselt number with no significant increase on the friction factor. Colgan et al. [43] tested a microchannel heat sink with strip fins and water cooling. They were able to dissipate heat fluxes of $400 W/cm^2$ while maintaining a pressure drop of 35 kPa. Lee et al. [10] examined another variety of sectional cuts, as they [10] manufactured a heat sink that has oblique sectional fins. The oblique fins work by interrupting and reducing the thickness of the boundary layer, keeping the flow in the developing region and therefore enhancing the

heat transfer. Lee et al. [10] were able to reach a heat transfer enhancement factor of 2.2 with little pressure drop penalty. Xie et al. [44] studied a microchannel with a combination of grooves and obstacles. Their results [44] showed that the combination of grooves and obstacles gave better heat transfer compared to an obstacle only microchannel. Gholami et al. [45] designed a microchannel heat sink with extended surfaces and triangular ribs. They concluded that adding a rib to the middle of the cross-sectional area of the microchannel contributes to the increase of the pressure drop and causes better distribution of the heat flux to the fluid.

Another method to increase heat transfer is to integrate a cavity to the microchannel. Xia et al. [46, 47, 48] did an extensive numerical study on a microchannel heat sink with triangular reentrant cavities. They [46] stated that the vortices in the cavities lead to chaotic advection which causes better mixing. The continuous interruption of the boundary layers enhanced the heat transfer in the microchannel. The same group also investigated the same geometry only adding an internal rib with different rib heights for Reynolds numbers between 150 to 600. They concluded the study by developing empirical correlations for the microchannel as a function of Re and the rib height [48].

1.1.3 Microchannels and Additive Manufacturing

The terms microfabrication and micromachining are associated with the manufacturing of the devices that have dimensions in the micrometer range [49]. Microchannels were initially manufactured using methods like lithography, and surface micromachining [1]. However, the demand for devices made from a variety of materials created a need for other manufacturing techniques to be developed. Examples of other manufacturing techniques used to create microchannels include electron beam machining, computer numerical control (CNC) ultra-

fine milling, as well as a method for creating high aspect ratio microstructures known by the German acronym LIGA [1]. Details on these and other techniques are described in [49]. Nevertheless, all of those manufacturing techniques suffer from geometric restrictions [50]. A microchannel design with curves or non-rectangular shapes can be extremely difficult or even impossible [50]. In addition, for microchannel heat sinks, a secondary lid is needed to seal the heat sink. Thus, additive manufacturing (AM) has recently emerged as a manufacturing method that can overcome the geometry restrictions. AM also has the ability to manufacture a single monolithic part. However, the number of studies and papers focused on the use of AM to fabricate microchannels using is small.

Stimpson et al. [51, 52] manufactured microchannel heat sinks for gas turbine engine components using direct metal laser sintering (DMLS), generally known as powder bed fusion. They manufactured 10 different test coupons all having rectangular cross-section with different aspect ratios and measured heat transfer and pressure drop at various flow conditions. The results showed that the friction factor for the channels with small hydraulic diameters changed significantly compared to channels manufactured traditionally. However, the heat transfer did not increase significantly with the increase in the friction factor. Snyder et al. [53] studied the effects of build direction and channel shape on microchannels. Their results indicate that the change in heat transfer is minimal with the build direction whereas the changes in pressure loss were significant with build direction. Kirsch & Thole [54] manufactured a microchannel pin fin heat sink using laser powder bed fusion and Inconel 718. They examined pressure drop and heat transfer for a total of four pin fin arrays with four different spacings over a range of Reynolds numbers, and for pressure drop and heat transfer. They found that with more pins added to the part, higher surface roughness was measured. The additively manufactured arrays had 20%-60% higher friction factors compared to traditionally manufactured fin pin arrays. Even though the friction factors were significantly higher,

the heat transfer did not change compared to traditionally manufactured pin fins. Kirsch et al. [55] studied the variation in the dimensions of the same parts using different materials and different builds for the laser powder bed fusion process. They showed that changing the build material can have significant effect on the geometry of the part produced. They also showed that changing the machine parameters of the DMLS process can change the produced geometry. Arie et al. [56] numerically studied a new microchannel heat exchanger design that can only be manufactured using additive. This study showed that using AM to fabricate complex designs such as manifolds and fins can improve the overall performance of the heat exchanger. They also stated that the complex design had a 60% increase in the gravimetric heat transfer density compared to a wavy fin heat exchanger and that higher printing resolution could lead to further improvements. Arie et al. [57] followed that numerical study with an experimental one that tested the same design. They were able to manufacture the part as a single unit using DMLS, with no fusing to combine the manifolds and the channels. The final part showed an average increase of 35% in heat transfer coefficient for the same pressure drop compared to the conventional wavy-fin design. They attribute this increase to the ability of AM to manufacture fins as thin as 150 μm and the complexity of the design. Dede et al. [58] manufactured a heat sink for jet impingement air cooling. The design of their heat sink was optimized and manufactured using AlSi12. They compared the optimized heat sink with a benchmark plate and pin-fin heat sinks, and they found that the optimized heat sink manufactured using additive manufacturing had higher coefficient of performance in both cases.

It can be seen from the literature review that the number of papers that utilize additive manufacturing to manufacture heat transfer devices, like heat sinks and heat exchangers, is limited, with even fewer papers focus on electronics cooling. In addition, most papers use the DMLS additive manufacturing process and the binder jetting process has not been

examined. The novelty of this thesis is the use of binder jetting additive manufacturing process to manufacture minichannel heat sinks for electronics cooling. The heat transfer performance of the heat sinks will be analyzed as well as the pressure drop across them. The applicability of using laminar flow theory for additively manufactured minichannel heat sinks will also be investigated.

Chapter 2

Geometric Characterization & Manufacturing Process

In this chapter, the geometry of the minichannel heat sinks is explained, along with the additive manufacturing process (binder jetting) chosen to manufacture them.

2.1 Geometric Characterization

Careful consideration to the geometry of the channel is vital for improving the performance of the heat sinks. A straight minichannel heat sinks was fabricated with a 0.8 hydraulic diameters. The straight channel design allows for a comparison between the manufactured part and established correlations. However, the straight channel design does not utilize the full power of additive manufacturing, but, it does serve as baseline step in future studies of minichannel heat sinks manufactured using binder jetting. Nevertheless, the manufactured heat sink does show one advantage of additive manufacturing in that it creates a monolithic part instead of having to subtractively manufacture the channels and then add a top lid to seal off the part. The design also takes advantage of additive manufacturing by have a square duct of right angles which is impossible to manufacturing traditionally.

Table 2.1 shows a detailed description of the manufactured heat sinks. All of the test heat sinks have an overall footprint area of: 25 mm x 35 mm. The dimensions chosen are not based

on increasing the heat transfer performance, or reducing the pressure drop penalty, rather they are based on the manufacturing constraints imposed by the binding jetting method. The simple design reduces the challenges associated with manufacturing small channels. Figures 2.1 & 2.2 show a front view of the minichannel heat sink and the flow path of the fluid. The square channels in this heat sink have dimensions of 0.8 mm x 0.8 mm.

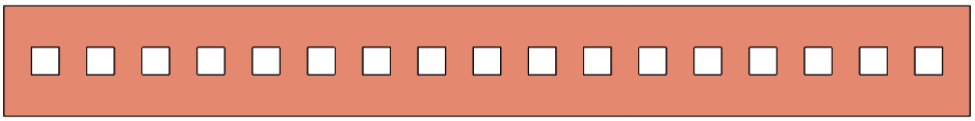

Figure 2.1: Front view of the minichannel heat sink with a hydraulic diameter of 0.8mm

Table 2.1: Specifications & dimensions of minichannel heat sinks

Channel shape	Material	Number of channels	Hydraulic Diameter (mm)
Rectangular	Stainless Steel 316 L	19	0.8

The heat sinks have a rectangular cross-sectional area, and based on previous published papers [24, 25, 26], the cross-sectional shape (circular, triangular, etc.) has a minimal effect on the performance of the minichannel heat sink. The minichannel heat sinks was manufactured using stainless powder, which shows one advantage of the binder jetting process compared to other powder additive manufacturing processes that are limited to using specific materials. The smallest minichannel heat sink has a hydraulic diameter of 0.8 mm and has a total number of 17 channels. The heat sink has a base ("wall" below the channels) was chosen to be 1.5 mm to avoid any possible leakage in the design. The walls between the channel are all 1 mm thick.

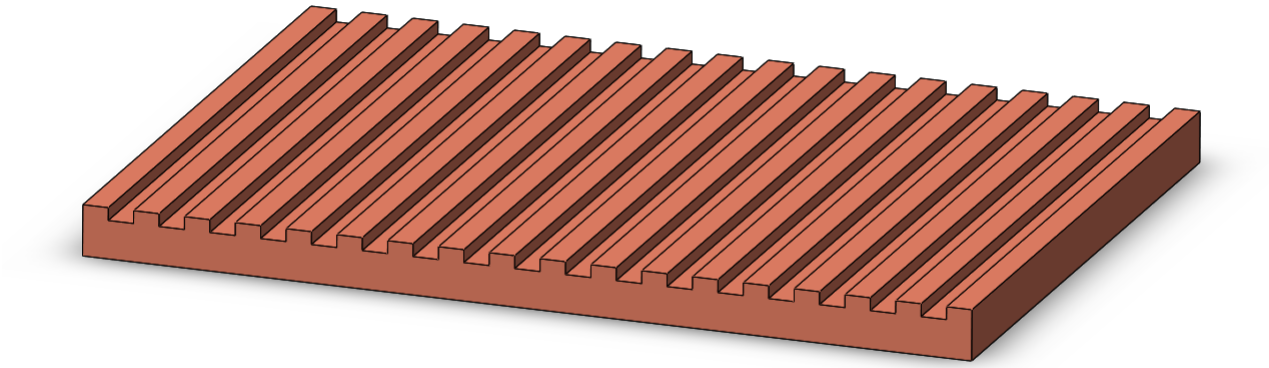

Figure 2.2: Cross sectional view of the minichannel heat sink with a hydraulic diameter of 0.8mm

2.2 Manufacturing Process

As previously stated, the binder jetting additive manufacturing process was used to manufacture the minichannel heat sinks. According to [59] there are seven different types of additive manufacturing techniques. The categorizes include: material extrusion, material jetting, binder jetting, powder bed fusion, direct energy deposition, vat polymerization, and sheet lamination. Each process has its unique advantageous and disadvantageous. The additive manufacturing market has grown rapidly in recent years, and the reason is partly due to the fact that additive manufacturing techniques are able to produce user-end final products [60].

Binder jetting is one of the techniques that shows great potential for manufacturing user end products in various industries [61, 62]. The way that this technique works is by injecting a binder from a print head to selectively choose a pattern from the powder bed. The bed is

lowered and another layer of the powder is sprayed and the binder continuous to the next layer until the part is completed. This produces a green part that requires two additional steps. One step is to remove the extra powder, usually by compressed air. In the second step, the part sintered in a hot furnace.

Binder jetting has many advantageous compared to other additive manufacturing techniques [63]. The use of a binder to generate geometry gives a wider ability of material selection, lower cost, and higher speed. The parts manufactured using binder jetting also experience lower residual stress compared to other metal additive manufacturing techniques, due to the fact that parts manufactured using binder jetting do not undergo direct melting of the part and do not experience rapid solidification. However, one major disadvantage of binder jetting is the lack of fundamental theoretical models that predict the part qualities. Therefore, there is always a significant amount of uncertainty with the properties of the printed parts [64].

Figure 2.3: ExOne machine used to manufacture parts. This system has a build box of 160x65x65mm

Chapter 3

Experimental Setup, Procedures, & Data Reduction

This chapter presents, a detailed description of the experimental setup along with a step-by-step explanation of the procedure for experiments. In addition, a section covers the data reduction and the correlations used in the analysis.

3.1 Experimental Setup

A minichannel heat sinks was experimentally characterized for thermal performance and pressure drop. Figure 3.1 shows the experimental loop for testing the heat sink.

First, water is drawn from a reservoir by a submerged water pump. The water pump used from Beckett Corporation (Figure 3.2) with a maximum capacity of 90 GPH, and a valve that controls the flow rate. In addition to circulating the coolant, the pump ensures that a constant flow rate is achieved even if the geometry of the heat sink has changed. The water reservoir is covered, and is maintained at ambient pressure and room temperature.

The water then passes through a three-way valve used to control the flow rate, then through a water flow meter. The flow meter (Figure 3.3) is Series VF Visi-Float from Dwyer Instruments with an accuracy of 3% of full scale. The water flow meter has a working range of

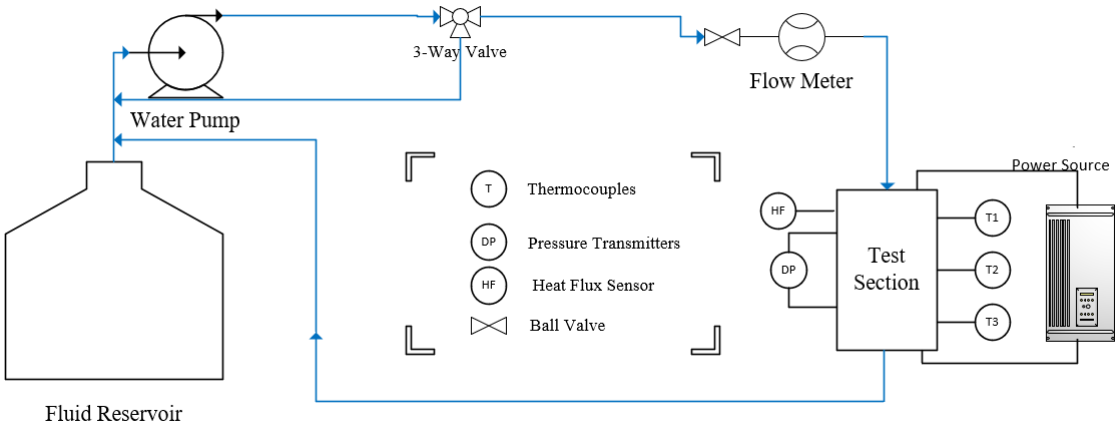

Figure 3.1: Schematic diagram of the experimental loop facility used to test the heat sinks. Thermocouples for temperature measurements are represented by T1, T2, and T3, whole DP denotes the pressure drop measurement across the heat sink and HF is the heat flux sensor.

1-20 GPH, and careful consideration for the installation of the flow meter was taken as it must be mounted in the vertical position in order to it to operate properly.

After passing through the flow meter, the coolant enters the test section. The test section (Figure 3.4)is manufactured through computer numerical control (CNC) machining. A block of Ultra-High Molecular Weight (UHMW) Polyethylene material was machined to the specified dimensions. A total of 16 holes were made on the block and the acrylic top for bolts to avoid leakage. Two 1mm diameter holes were drilled on the side of the block to insert thermocouples. On the acrylic top, two 1/4" diameter holes were made to insert the pressure sensors. The overall dimensions of the assembly were: 4x5.9x1.25 inches.

Th heat sinks were placed at the center of the UHMW holder for testing. A polyimide heater was attached to the bottom of the heat sink to supply heat, and a variable DC supply was used to control the input.

A heat flux sensor was placed between the heater and the heat sink. The sensor, shown in Figure 4.3, is 380 microns thick and has a heat flux range of +/- 150 kW/m^2. The heat flux

Figure 3.2: Pump used to circulate water from the reservoir and through the loop

sensor also has an embedded surface thermocouple. A flat thermocouple is used to measure the surface temperature, as it reduces the contact resistance between the surface of the heat sink and the thermocouple, Figure 3.8.

On the sides of the UHMW holder, small holes were made to insert two ball T-type thermocouples (Omega, 5TC-TT-T-30-36) to measure the bulk temperature of the water. The thermocouples are 0.25 mm in diameter and have a polymer PFA coating for insulation.

The acrylic top contains two holes for the pressure transducers. The pressure sensor (Dwyer Instruments, 629C-01-R1-P1-E1-S3-LCD), shown in Figure 3.9, monitors the pressure drop across the heat sink. It uses dual pressure sensors that convert the pressure changes to a voltage signal. The pressure transducer has an accuracy of 0.5% of full scale, and a working range of 0-5 psi differential (psid). The pressure sensors are placed immediately before and after the heat sink to avoid minor pressure losses. After the heat sink is placed in the testing apparatus, the assembly is closed by 16 bolts and nuts. Below the heat sink, a polyimide heater supplies heat, and attached to it a heat flux sensor that records that heat flux into the heat sinks. Between the heat flux sensor and the heat sink is the flat thermocouple.

Figure 3.3: Dywer water flow meter. The flow meter has a working range 1-20 GPH and accuracy of 3% full scale

Figure

The steady-state readings from the thermocouples and the pressure transmitters were recorded and store by a computer, and a LabVIEW code was used to receive and translate the signals. Figure 3.12 shows the block diagram of the code used in LabVIEW.

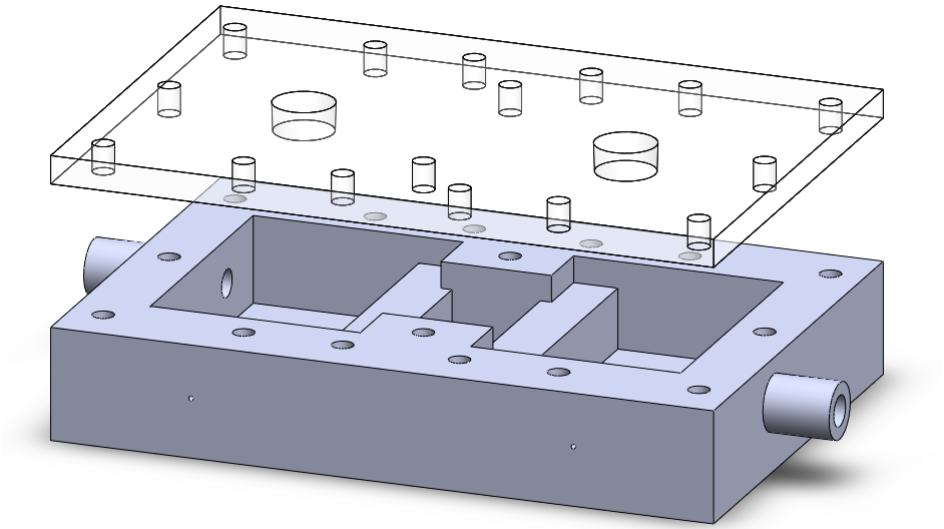

Figure 3.4: UHMW Polyethylene holder and acrylic top assembly. A total of 16 holes for bolts to avoid leakage. Two 1/4" holes on the acrylic piece to mount the pressure transmitters, and 1mm holes on the sides for the thermocouples.

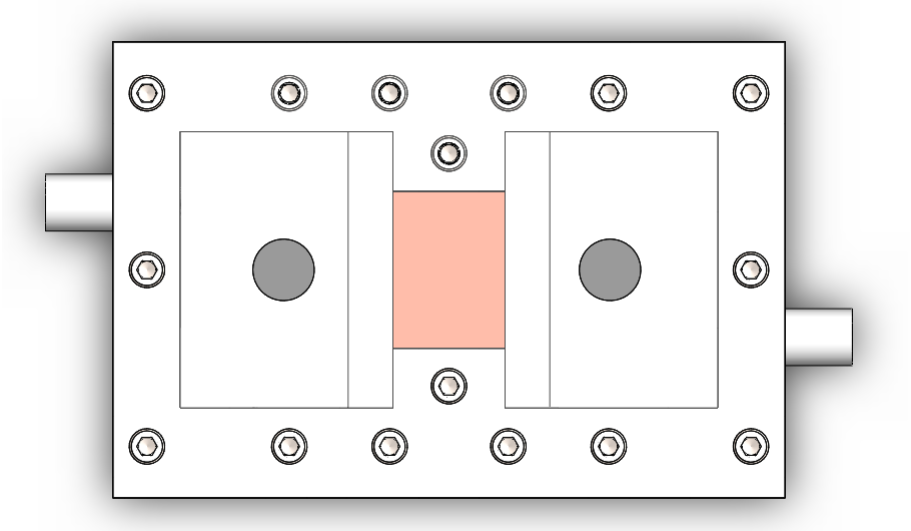

Figure 3.5: Top view of the experimental holder

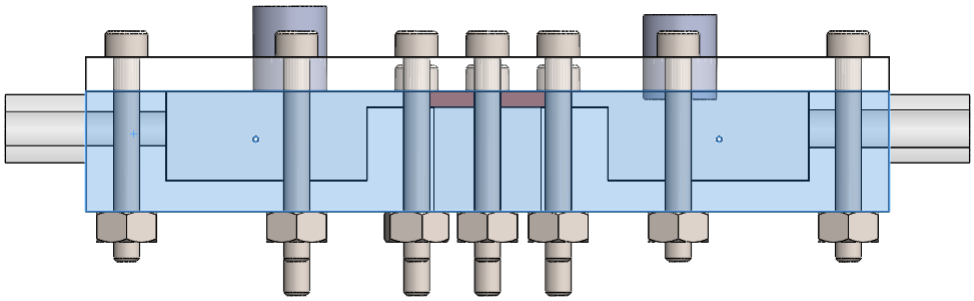

Figure 3.6: Side view of the experimental holder

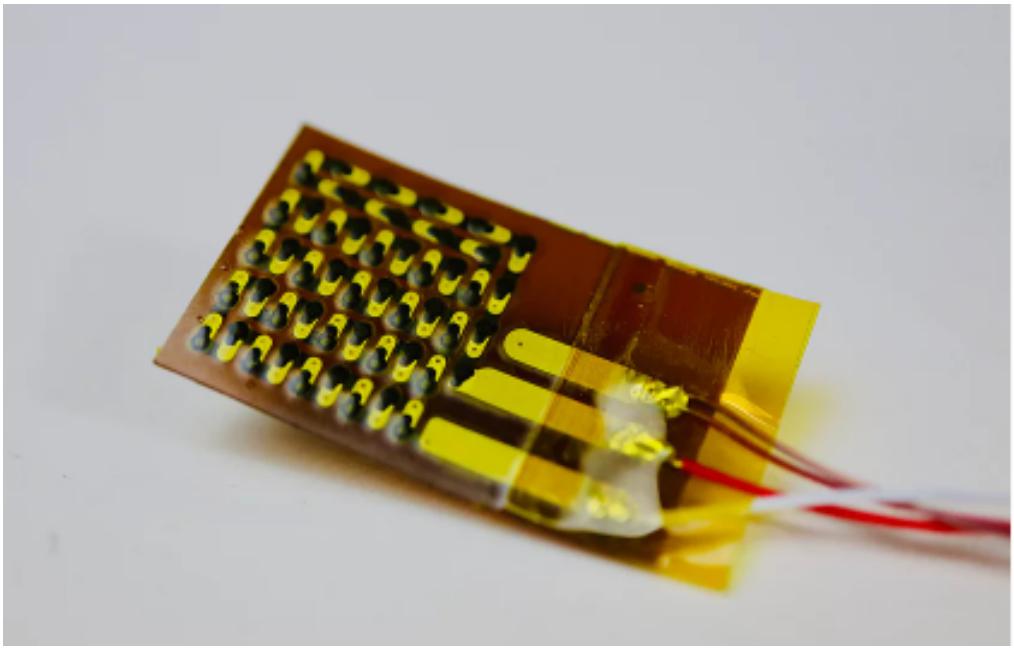

Figure 3.7: Heat flux sensor (Fluxteq PHSF-OEM) placed below the heater. It has a thickness of 380 microns.

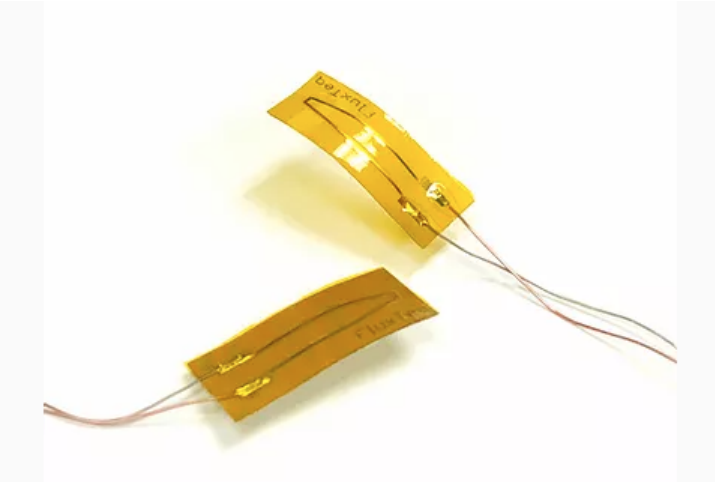

Figure 3.8: Thermocouple used in experiment.

Figure 3.9: Pressure transmitter used to measure the pressure drop across the minichannel heat sink. The pressure range is 0-5 psid.

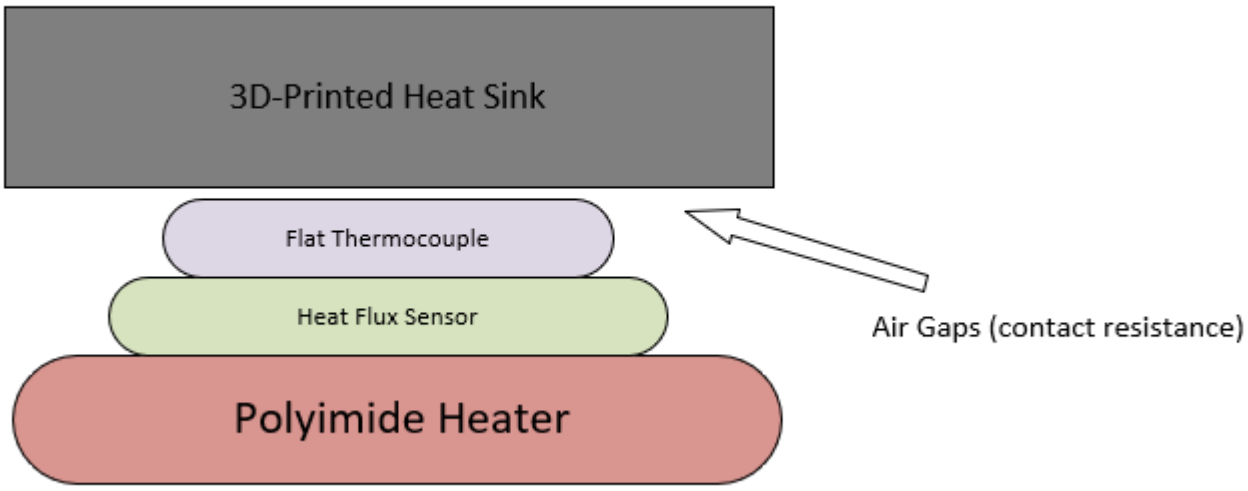

Figure 3.10: Schematic diagram of the assembly of sensors below the heat sink.

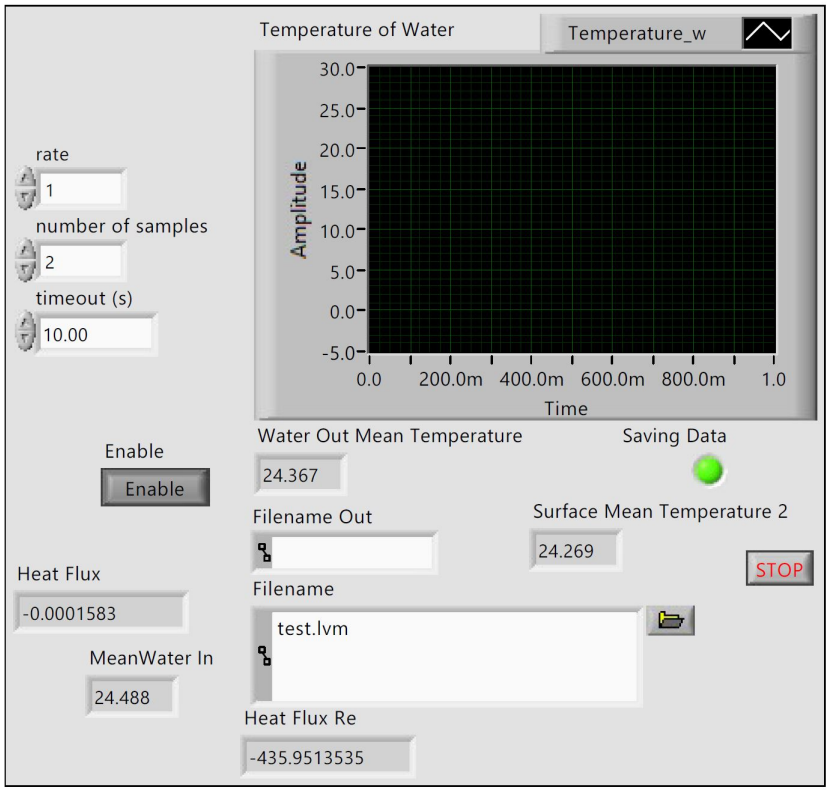

Figure 3.11: LABVIEW interface used to acquire the pressure drop and thermocouple readings.

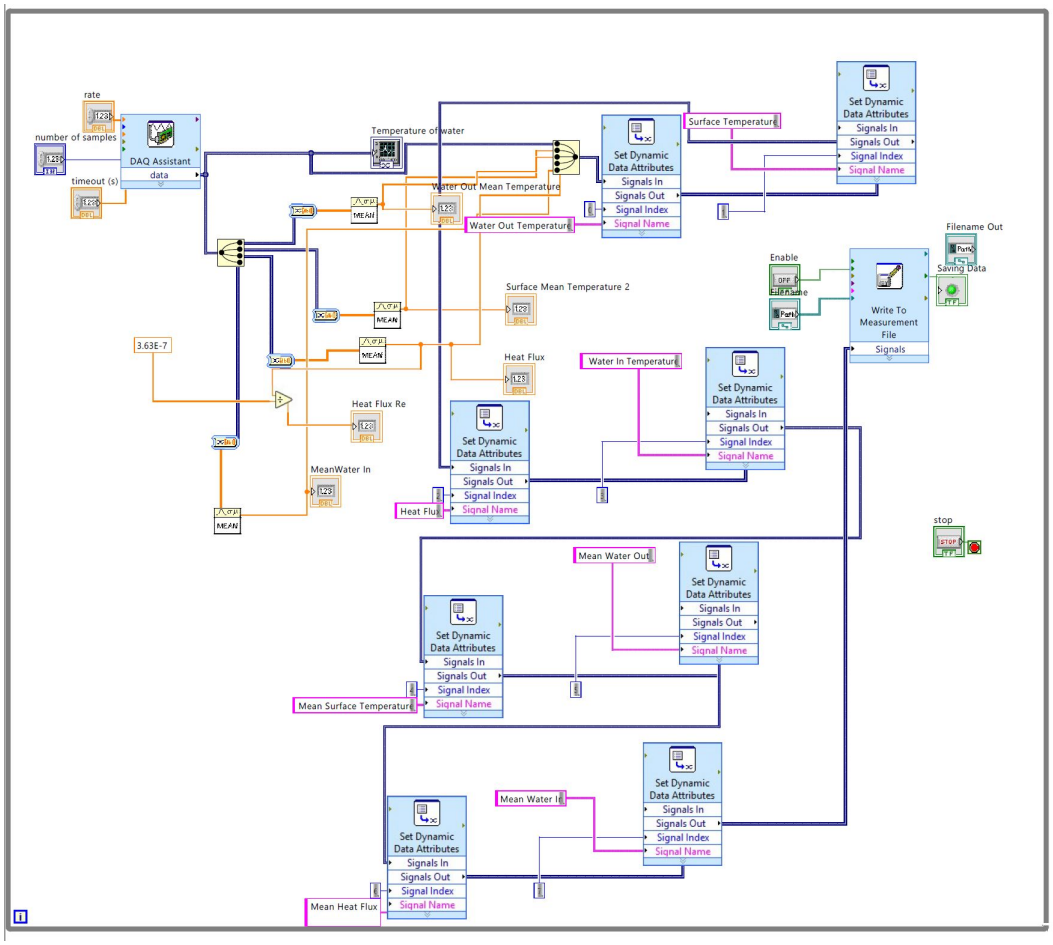

Figure 3.12: LABVIEW block diagram code used to acquire the pressure drop and thermocouple readings.

3.2 Test Procedures

The test procedure to characterize the thermal and hydraulic performance of the heat sink is summarized in the following points:

- Before the test begins, the flow is allowed to continue for several minutes to remove any loose particles inside the heat sink, and check for leaks, and high flow rates are used in this step.

- To characterize the hydraulic performance, the flow rate through the microchannel (unheated) is changed from 100 ml/min to 1200 ml/min, in increments of 100 ml/min, during which the pressure drop measurements are recorded at steady-state using the pressure transmitter.

- For heat transfer measurements, the power input is set at $5000 W/m^2$ and $6500 W/m^2$. The heat transfer is measured at the same flow rate increments as the pressure drop measurements. During this step, two bulk thermocouples measure the inlet and the outlet temperature of the water, and one surface thermocouple records the surface temperature of the heat sink. Also, the heat flux sensor measure the heat input to the heat sink.

3.3 Data Reduction

This section, a detail description of the data analysis.

3.3.1 Pressure Drop & Friction Factor Analysis

The friction factor across the heat sink is calculated using the Darcy equation 3.1:

$$f = \frac{2D_h \Delta P}{\rho u^2 L_c} \tag{3.1}$$

where D_h is the hydraulic diameter, ΔP is the pressure drop that is measured directly from the pressure transducer, ρ is the density of the fluid, u is the velocity of the fluid, and L_c is the length of the channel. The poiseuille number is the product of the friction factor and the Reynolds Number and can be computed after calculating the friction factor.

The friction factor values can be compared to literature correlations. Shah et al. [65] presented a correlation for the friction factor for fully developed laminar flow in a rectangular duct:

$$f_{F,fd} = (\frac{24}{Re})(1 - 1.3553\alpha + 1.9467\alpha^2 - 1.7012\alpha^3 + 0.9564\alpha^4 - 0.2537\alpha^5) \tag{3.2}$$

where α is the aspect ratio, which is defined as $\alpha = H_{channel}/W_{channel}$. The constraint of the previous equation is that the aspect ratio must be less than one. If the aspect ratio was greater than 1, the inverse has to be taken and used in the equation.

Nevertheless, Equation 3.2 deals with a fully developed flow. The flow in minichannels can be dominated by developing lengths because of the short channel lengths [66]. The non-dimensional flow distance is used to determine if the flow is developing or fully developed is given by [66]:

$$x^+ = \frac{x}{D_h Re} \tag{3.3}$$

Where x is the location along the axial flow direction. The flow is assumed fully developed

when $x^+ = 0.05$. Therefore, another correlation is needed to truly capture the friction factor in the developing region. Steinke & Kandlikar [66] showed that for a friction factor in a developing flow region, could be determined by:

$$f_{F,dev} = \frac{K_\infty D_H}{4L_{dev}} + f_{F,fd} \tag{3.4}$$

where $L_{dev} = 0.05Re * D_H$ and K_∞ is the Hagenbach factor and is equal to (for rectangular ducts):

$$K_\infty = 0.6796 + 1.2197\alpha + 3.38089\alpha^2 - 9.5921\alpha^3 + 8.9089\alpha^4 - 2.29959\alpha^5 \tag{3.5}$$

3.3.2 Heat Transfer Analysis

For heat transfer analysis, the heat transfer coefficient has to be calculated using Equation 3.6:

$$h = \frac{Q}{NA_s(T_{wall} - T_m)} \tag{3.6}$$

where Q is the amount of heat that goes through the heat sink, N is the number of channels, A_s is the wetted surface area that is equal to:

$$A_s = L_{channel} * (w + 2\eta_{fin}L_{fin,c}) \tag{3.7}$$

where $L_{channel}$ is the length of the channel, w is the width of the channel, η is the fin efficiency of the channel walls and $L_{fin,c}$ is the corrected height of the channel. T_m is the mean fluid temperature and is calculated using:

$$T_m = \frac{T_{in} + T_{out}}{2} \tag{3.8}$$

where T_{in} is the inlet water temperature, and T_{out} is the outlet water temperature. On the other hand, T_{wall} in Equation 3.6 represents the temperature of the bottom surface of the heat sink. To calculate η, it is assumed that the walls of the channel act like fins with adiabatic tip conditions, and corrected fin length of 1.5 of the height of the channel to account for the four-sided conduction around the channel. This approach has been tried by previous researchers [49] and it differs from other experiments where the heat sinks are manufactured traditionally and a cover lid from an insulating material is placed on the top. To calculate η the following is used:

$$\eta_{fin} = \frac{tanh(mL_{fin})}{mL_{fin}} \tag{3.9}$$

$$m = \sqrt{\frac{h * P_{fin}}{k_s * A_{fin}}} \tag{3.10}$$

where P_{fin} is the perimeter of the fin and k_s is the thermal conductivity of the metal. Here, it is assumed that the thermal conductivity of the 3D printed material is the same as the bulk material. Nevertheless, because of the small channel size, measuring the surface temperature is challenging, and instead, the bottom surface temperature is measured and Fourier's Law is used to determine T_{wall}:

$$T_{wall} = T_{bottom} - Q^{"} * R_{total} \tag{3.11}$$

where $Q^{"}$ is the heat flux into the heat sink and is measure using a heat flux sensor, and R_{tot} is the total thermal resistance per unit area between the flat thermocouple (shown schematically in Fig 3.10) and the wall of the channel. The total resistance is extremely important, as small variations in the resistance will alter the results of the experimentally measured convection heat transfer coefficient drastically. The thermocouple used is encased

in a Kapton film that has to be accounted for. In addition, the contact resistance between the Kapton and the stainless steel surface adds significantly to the total resistance, therefore the total resistance between the thermocouple and the channel wall becomes:

$$R_{total} = \frac{t_{kapton}}{K_{kapton}} + R_{c,t} + R_{conduction} \tag{3.12}$$

where $R_{conduction} = t_{base}/K_{metal}$, and t_{kapton} is the thickness of the Kapton tape. The contact resistance is difficult to determine as it is a function of the actual area of contact between the materials, and this area of contact is a function of pressure holding the materials together. The resistances are best illustrated using a circuit resistance shown in Figure Once the convection heat transfer coefficient has been determined, the Nusselt number can then be calculated using:

$$Nu = \frac{hD_H}{k_{liquid}} \tag{3.13}$$

where k_{liquid} is the thermal conductivity of the water, and D_H is the hydraulic diameter of the minichannel and is equal to:

$$D_H = \frac{4w * H}{2(w + H)} \tag{3.14}$$

where w is the width of the channel, and H is the height of the channel. The Nusselt number

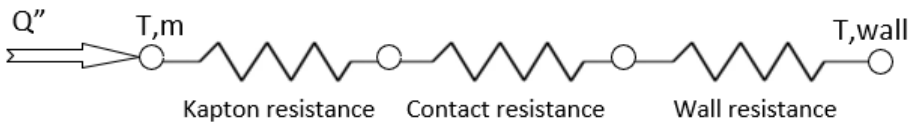

Figure 3.13: Thermal resistances network between the thermocouple and the channel wall.

calculations can be compared to well established correlations in the literature. Lee and

Garimella [67] recently developed a correlation for thermally developing flow in a rectangular duct with constant heat flux conditions:

$$Nu_{ave} = \frac{1}{C_1(x^*)^{C_2} + C_3} + C_4, \ for\ 1 \leq \alpha \leq 10 \tag{3.15}$$

where:

$$C_1 = (-2.757E{-}3)\alpha^3 + (3.274E{-}2)\alpha^2 - (7.464E{-}5)\alpha + 4.476$$

$$C_2 = 6.391E{-}1$$

$$C_3 = (1.604E{-}4)\alpha^2{-}(2.622E{-}3)\alpha + (2.568E{-}2)$$

$$C_4 = 7.301{-}(1.311E1)\alpha^{-1} + (1.519E1)\alpha^{-2}{-}6.094\alpha^{-3}$$

The correlation is applicable when $x^* < 0.05$ where x^* is equal to:

$$x^* = \frac{L}{D_H Re\ Pr} \tag{3.16}$$

Beyond 0.05, the flow can be considered fully developed, and the following formula can be used [68]:

$$Nu = 8.235(1 - \frac{2.0421}{\alpha} + \frac{3.0853}{\alpha^2} - \frac{2.4765}{\alpha^3} + \frac{1.0578}{\alpha^4} - \frac{0.1861}{\alpha^5}) \tag{3.17}$$

In the following measurements, it can be seen that these experiments fall into the regime where the previous correlation would apply, the developing region.

Chapter 4

Results & Discussion

4.1 Manufacturing Results & Guidelines

The first attempts to manufacture the heat sink were done with binder jetting using copper powder. The copper particles had an average size of $5\mu m$, and three designs with different hydraulic diameters were attempted. Unfortunately, the fine powder size coupled with the small hydraulic diameter caused all of the prints to fail during the depowdering step. Figures 4.1 & 4.2 show the failed samples and the cracks that resulted from depowdering. These results show that there are still some significant challenges when trying to print small features using fine powder. Therefore, as a general guideline, small features should be avoided when manufacturing samples using extremely fine powder and binder jetting. Alternatively, the heat sink was finally manufactured using a commercial company (ExOne). The chosen material was Stainless Steel 316 L, and the final sample shown in Figure 4.3.

An Archimedes test was performed to measure the density of the final printed part. According to the manufacturer, the final density of the part should be around 98%. However, from our experimental measurements we found that the relative density of the samples had an average of 82%. This lower density would reduce the thermal conductivity of the material slightly which also reduces its stability for liquid cooling for electronics. Methods to increase the density should be further investigated. A detailed description of the dimensions of the printed samples (with $D_h = 1.25$ & $D_h = 1.5$) are shown in Table 4.1.

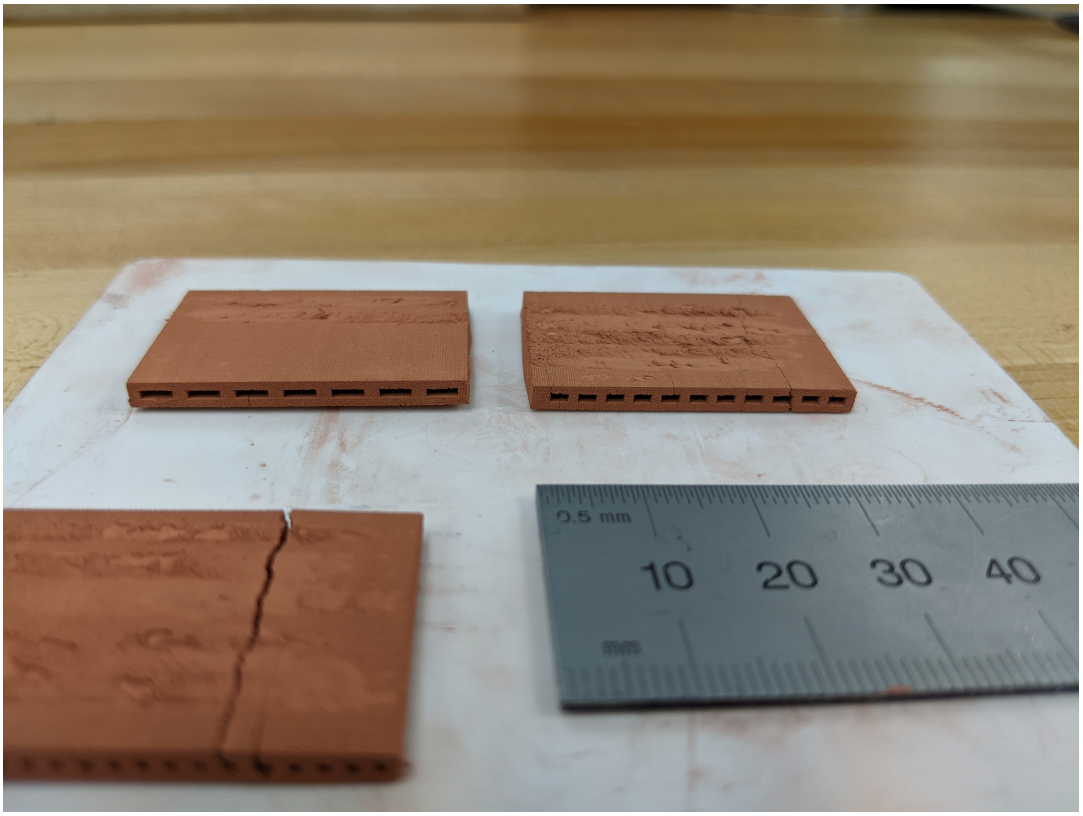

Figure 4.1: The failed copper samples. Cracking occurred during the depowdering step of the manufacturing process.

Table 4.1: Dimensions of the final printed samples

Sample	Width (mm)	Length (mm)	Thickness (mm)	Volume (mm^3)	Mass (g)
1	34.79	25.02	2.98	609.4872	15.0351
2	34.94	25.02	2.93	569.7054	15.4419

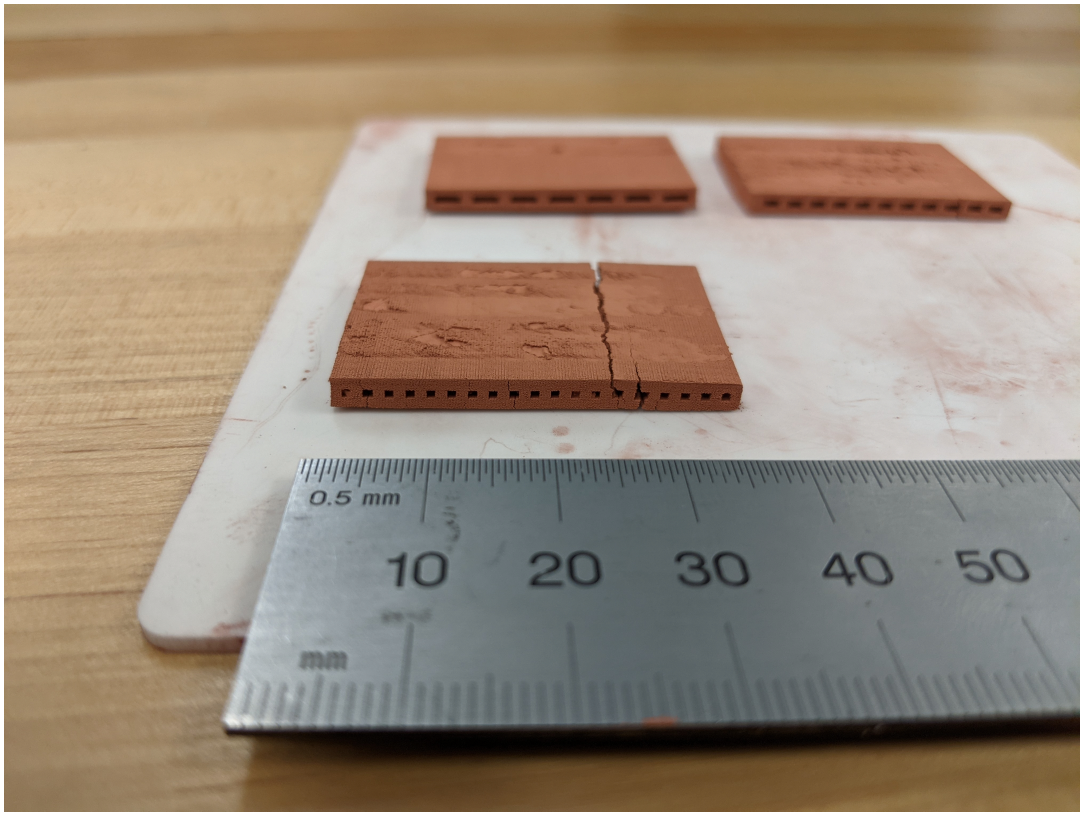

Figure 4.2: A second view of the failed copper samples. Cracking occurred during the depowdering step of the manufacturing process.

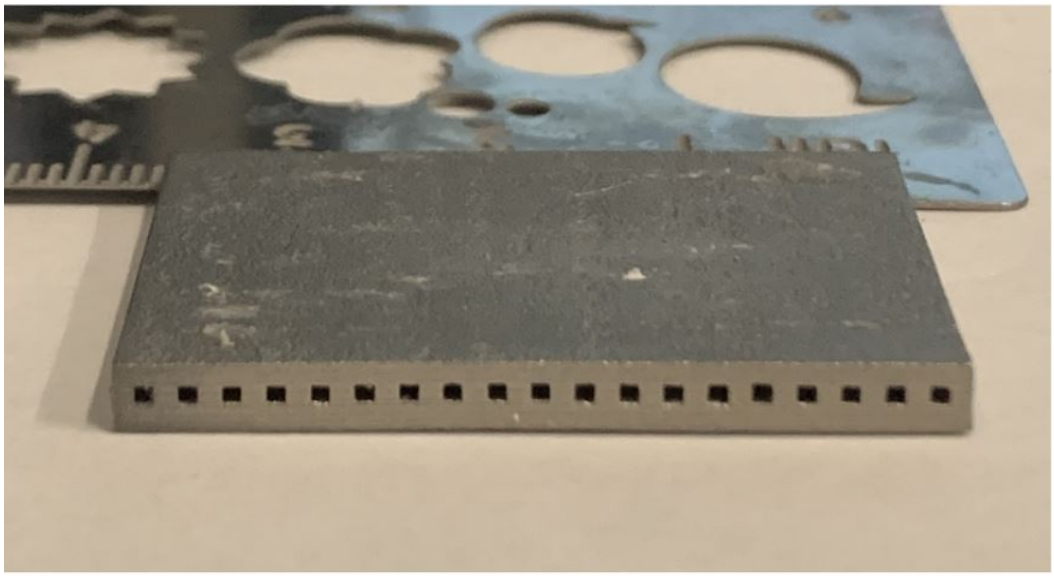

Figure 4.3: Tested Sample. Manufactured from Stainless Steel 316 L by ExOne.

4.2 Hydraulic Results

Figure 4.4 (Using equation 3.3) shows the developing length (or entrance length), which is the distance a flow travels before it becomes fully developed, as a function of the Reynolds number. It can be seen that, except at the lowest Reynolds numbers, the flow is expected to be dominated by the developing region for the heat sink examined in this work. Therefore, in order to accurately evaluate the performance of the heat sink, the appropriate correlations for developing flow must be used.

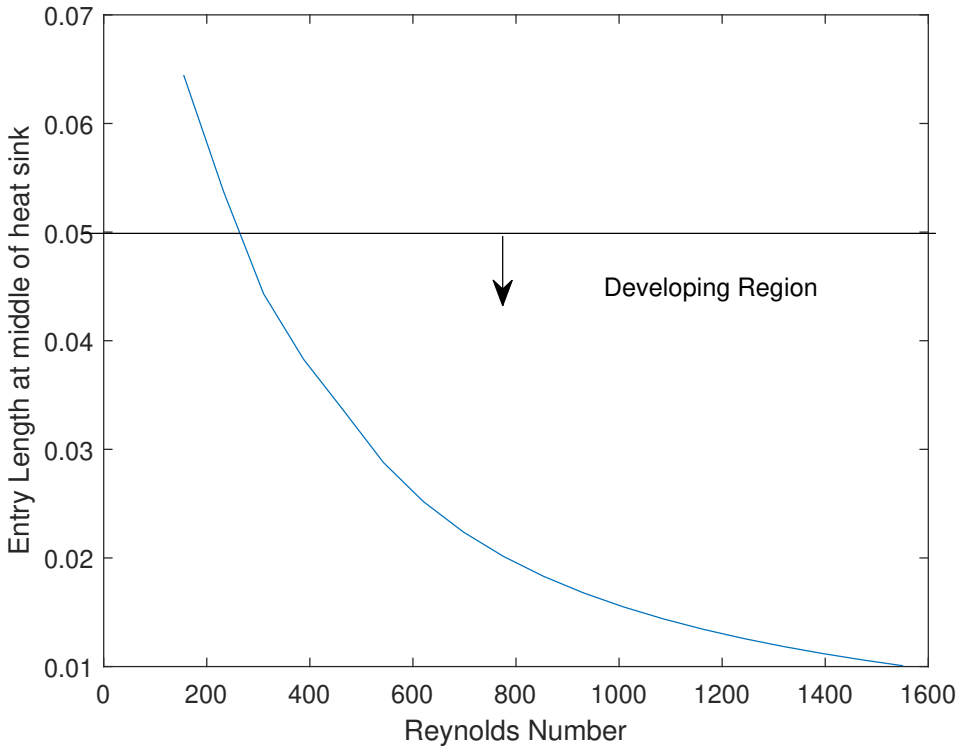

Figure 4.4: The non-dimensional flow distance as a function of the Re number. Note that the flow is dominated by the developing region, except at the lowest Re value.

Figure 4.5 shows the experimentally measured friction factor of the minichannel with $D_h = 0.8mm$ as a function of the Reynolds number. The friction factor of the minichannel matches the behavior of the conventional channel for internal flow. As Reynolds number increase, the

friction factor decreases steadily. Comparing the experimental results with the correlation 3.4, it can be noticed that the results starts deviating at around 500 Reynolds number. This deviation signals that the flow is transitioning to turbulence. The early transition can be attributed to the surface roughness associated with the additive manufacturing process. Collins et al. [50] have reported a similar observation as they had a transition value of Re=500. Figure 4.6 shows a comparison between the results. The early transition to turbulence can also be seen in many other papers [50, 69].

Figure 4.7 shows the pressure drop across the heat sink as a function of the Reynolds number. Note the change in the slope of the function at around Re=400. This also agrees with the previous analysis that the minichannel exhibits an early transition to turbulence, and the added surface roughness from the manufacturing process narrows the range of the laminar region. The agreement between the experimental measurements and the correlation at the laminar flow region indicates that the manufacturing process was able to produce a near net shape geometry of the heat sink. In addition, the early transition to turbulence should be considered in future designs of heat sinks as most analysis assume that the heat sink is working in the laminar region.

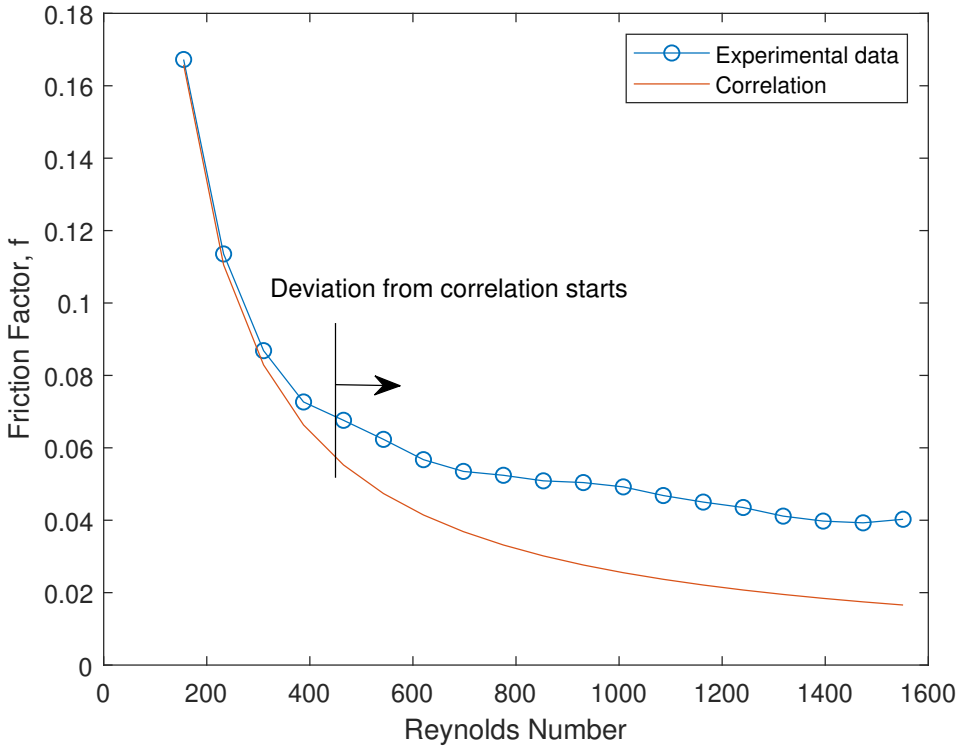

Figure 4.5: Friction factor as a function of Reynolds number for minichannel with $D_h = 0.8$. Notice the flow starts deviating from the correlation at a critical Reynolds number of 500.

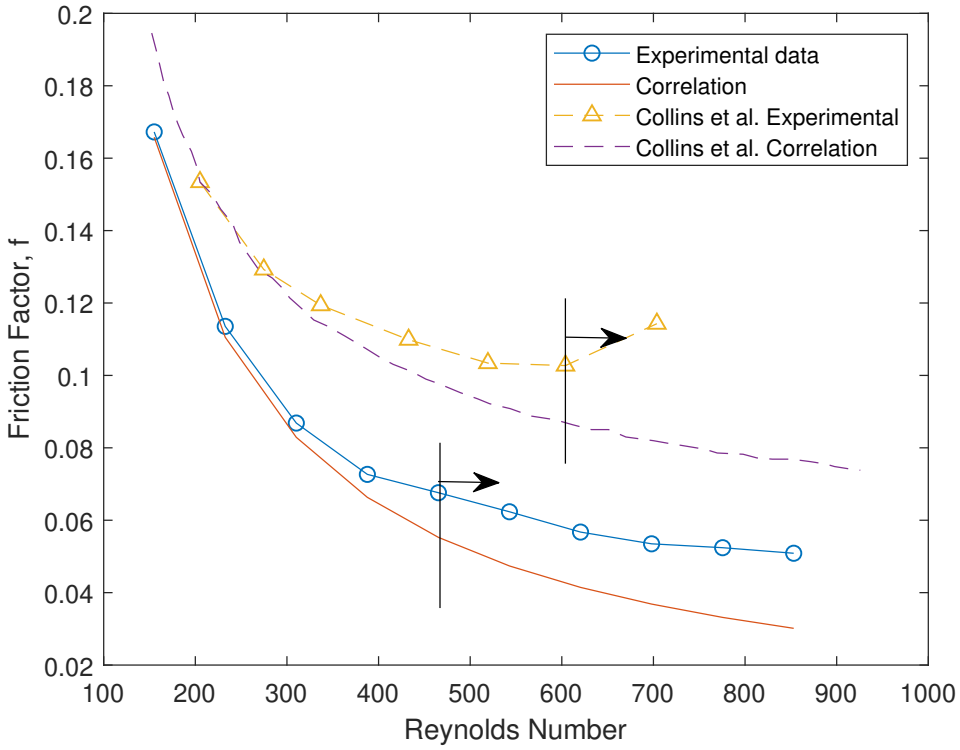

Figure 4.6: Friction factor as a function of Reynolds number comparison with Collins et al. Notice the flow starts deviating from the correlation at a critical Reynolds number of 500.

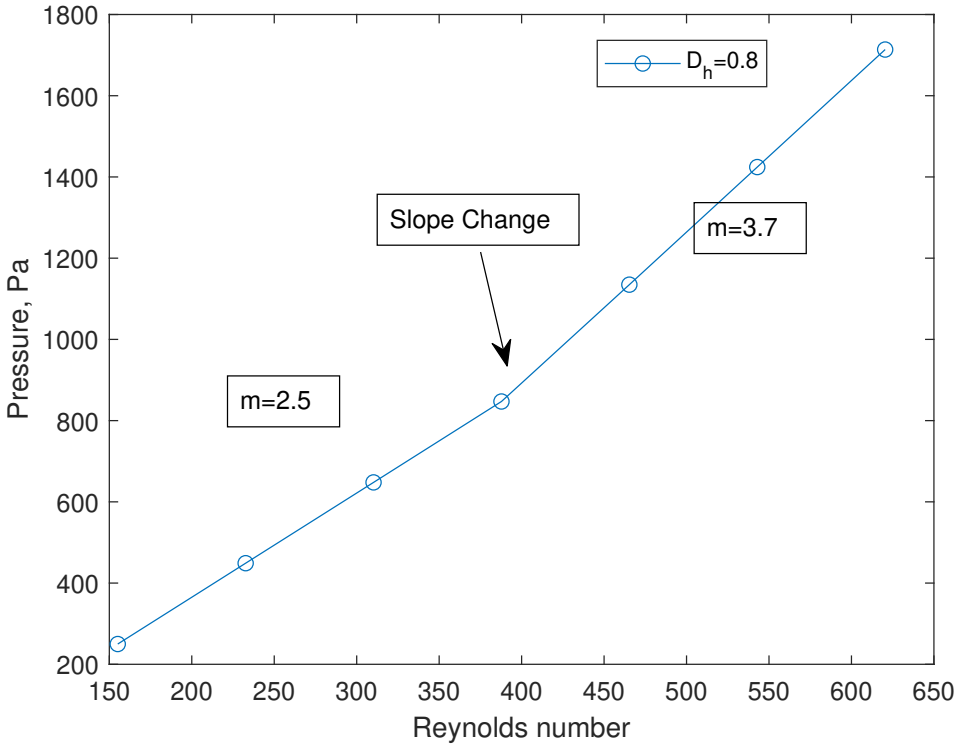

Figure 4.7: Pressure drop across the heat sink as a function of Reynolds number. Note the slope change at about Re 500.

4.3 Thermal Results

The minichannel with a hydraulic diameter of 0.8 mm was tested for thermal performance. For those experiments, the contact resistance was initially estimated to be a value of $0.0009 m^2 K/W$. The average heat transfer coefficient as a function of the Reynolds number in Figure 4.8. A total of three different experiments were attempted at two different heat flux conditions, $5000 W/m^2$ and $6500 W/m^2$. From the graph it can be noted that the highest error on different heat flux experiments is around 4%.

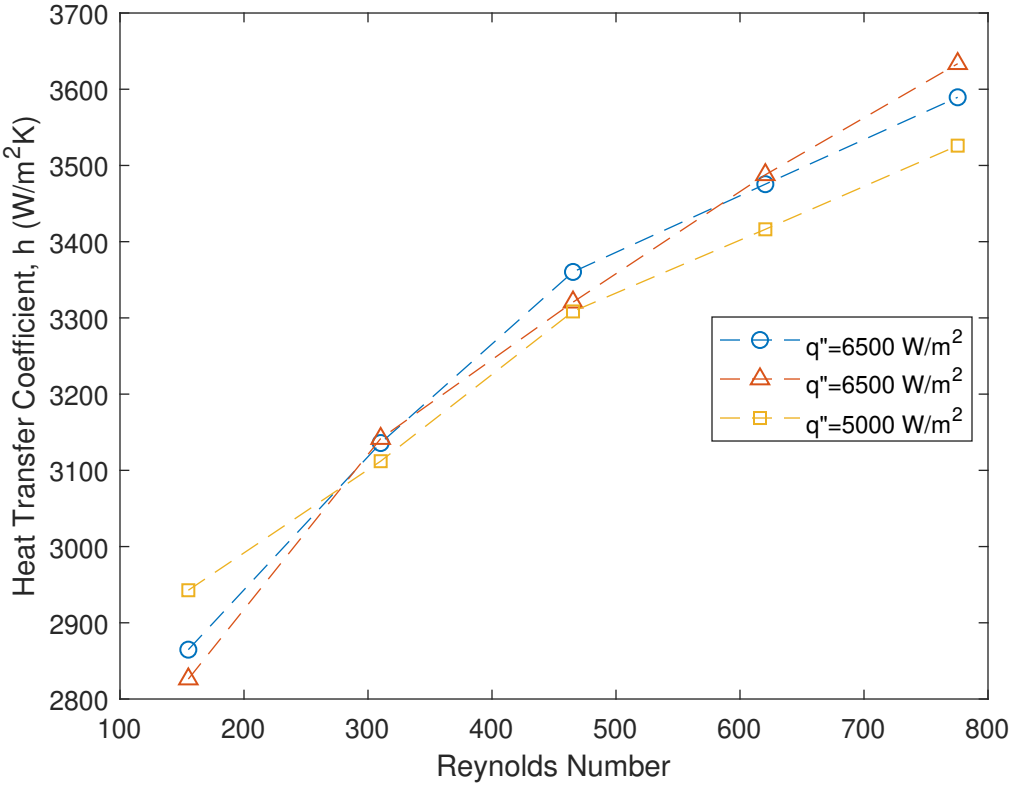

Figure 4.8: Heat Transfer coefficient as a function of the Reynolds number. The maximum difference for repeatability is 4%

Comparing the results with Rastan et al. [70], Figure 4.10, the 0.8 mm channel had a higher average heat transfer coefficient. However, Rastan et al [70] used an additively manufactured

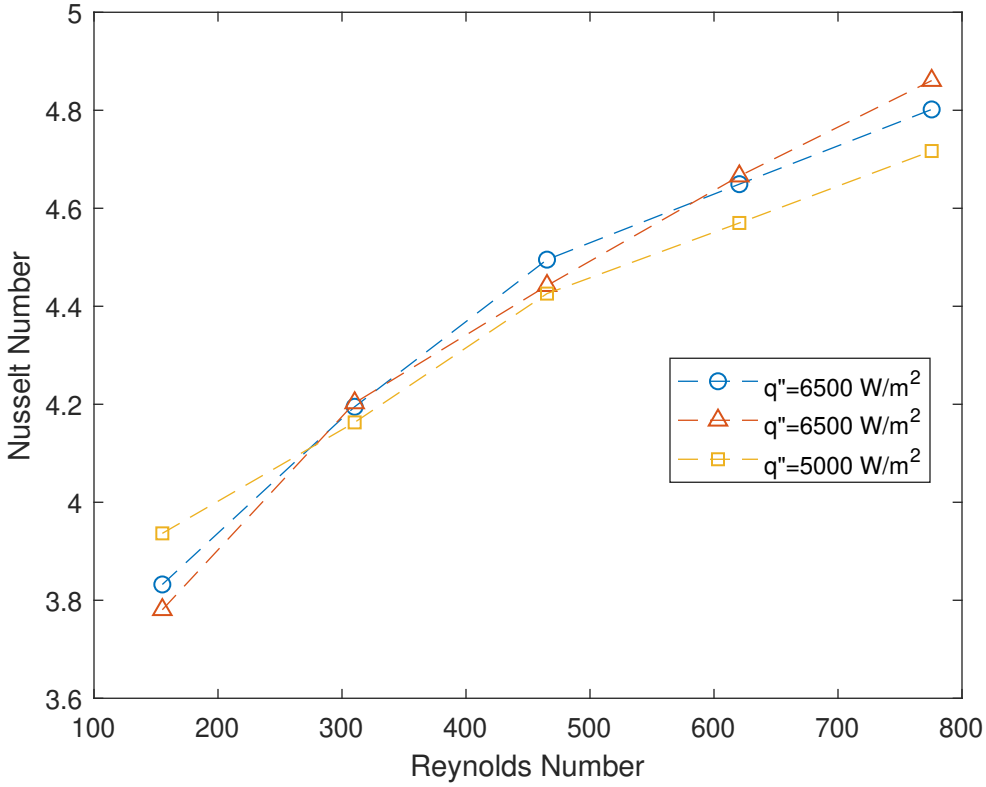

Figure 4.9: Nusselt number as a function of the Reynolds number. Maximum difference on repeatability is 4%

heat sink made from aluminum alloy (AlSi10Mg) with a larger hydraulic diameter, 2.4 mm. Therefore, the increase in h can be attributed to the smaller channel and the bigger surface area.

The thermal results can be compared to an established correlation 3.15. Figure 4.11 shows the Nusselt number of the experimental value and the correlation values. It can be seen that there is a mismatch between the two values. Further investigation is needed to address the mismatch, however, it might be attributed to the uncertainty in the value of the contact resistance. Also, due to the experimental sample holder, the first and last 2 mm of the channels are not heated, this might also contribute to the deviation between the experimental results and the correlation.

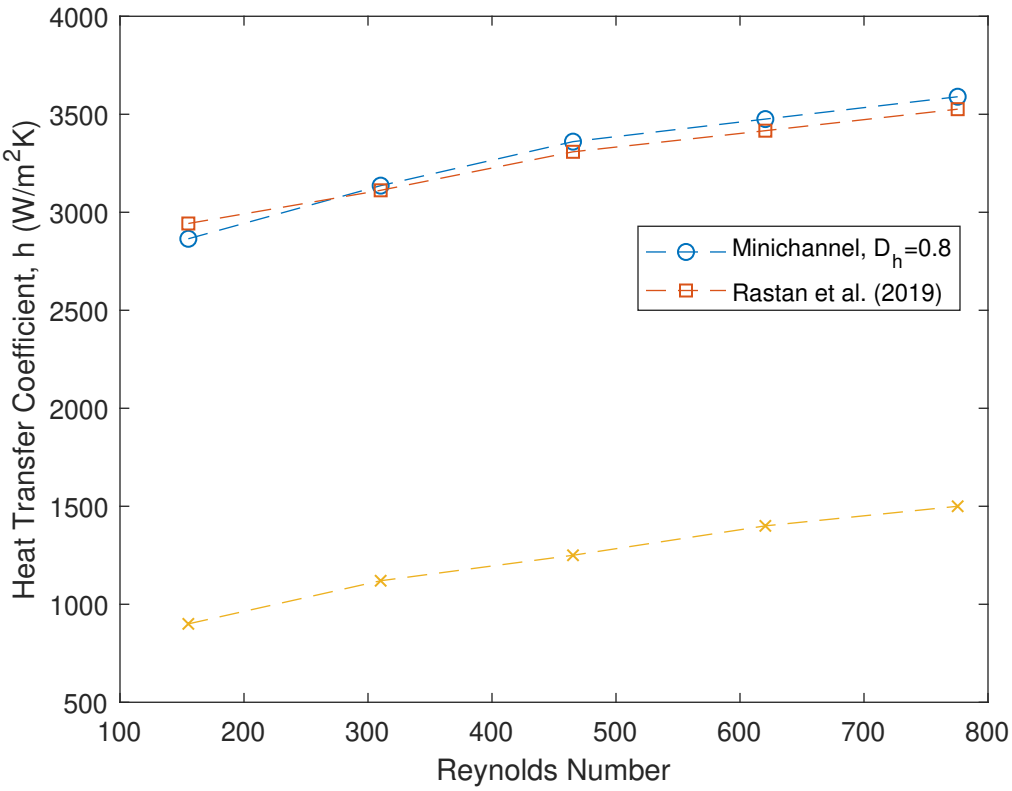

Figure 4.10: Comparison between Rastan et al. and the minichannel tested in this study.

4.3.1 Thermal results and the contact resistance

In the previous analysis, the contact resistance was estimated to be a value of $0.0009 m^2 K/W$. However, further investigation is needed to accurately determine this value. Figure 4.12 shows the effect of the contact resistance on the heat transfer coefficient. It can be seen that a small change in the contact resistance can lead to large changes in the convection heat transfer coefficient. Figure 4.13 shows the effect of the contact resistance on the Nusselt number. Examining the figure, it can be seen that the convection heat transfer coefficient value diverges when the contact resistance exceeds a value of $0.0009 m^2 K/W$. Therefore, that value was chosen in all analyses. Further investigation is required to accurately determine the contact resistance value. A transient model that works on calculating the resistance has

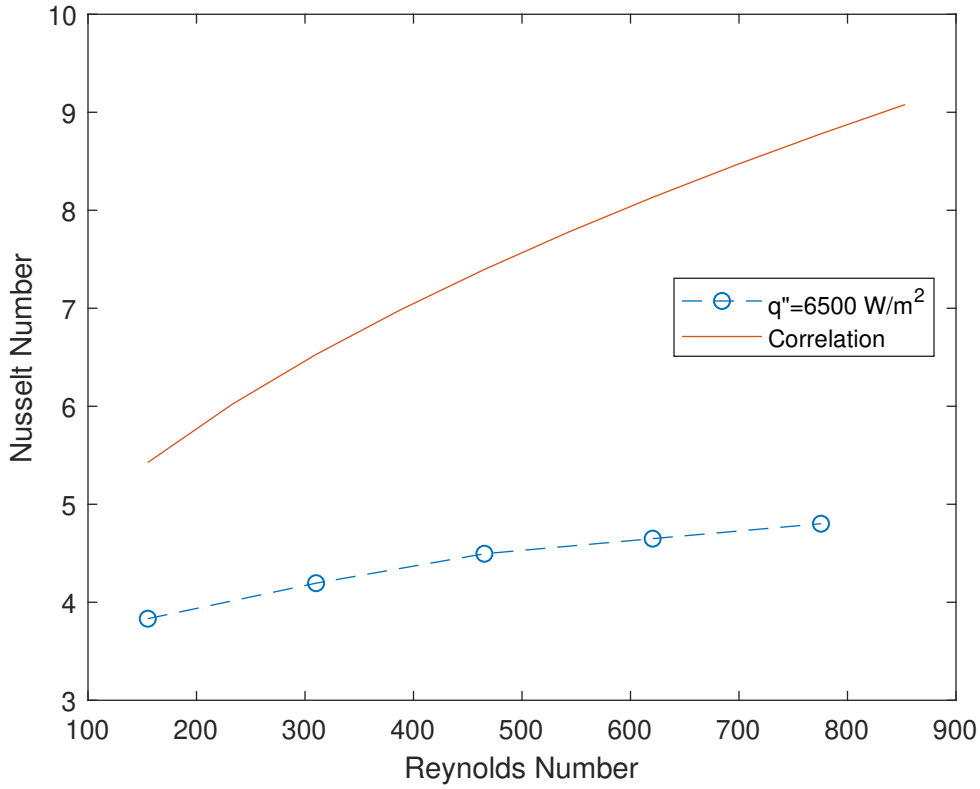

Figure 4.11: Nusselt number as a function of Reynolds number. It can be seen that there is a significant mismatch between the measured values and the experimental values.

been developed in the lab previously and might be used. Other methods that can eliminate the contact resistance is drilling holes inside the heat sink and inserting a thermocouple, or manufacturing a new sample that has a built-in hole to insert a thermocouple.

4.3.2 Thermal results and the heat flux

Referring back to Figure 4.8 it can be seen that the heat transfer coefficient does not change significantly when the heat flux increases from $5000W/m^2$ to $6500W/m^2$. However, where reducing the heat flux to $3000W/m^2$, it can be seen that the heat transfer coefficient changes significantly, as shown in Figure 4.14. These results indicate that the experimental set up

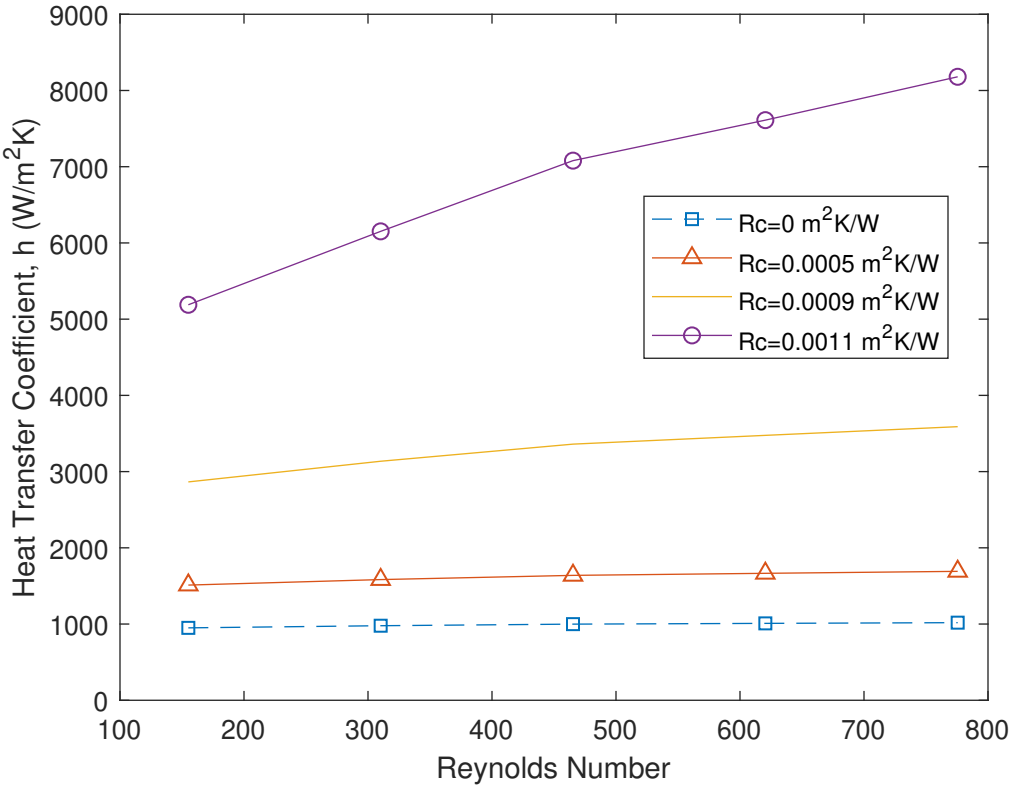

Figure 4.12: The change in the heat transfer coefficient as the contact resistance changes.

has a lower limit for it to yield good results. In this case, the limit is around $5000W/m^2$. In order to test at a lower heat flux, higher sensitivity equipment and better contact resistance should be achieved.

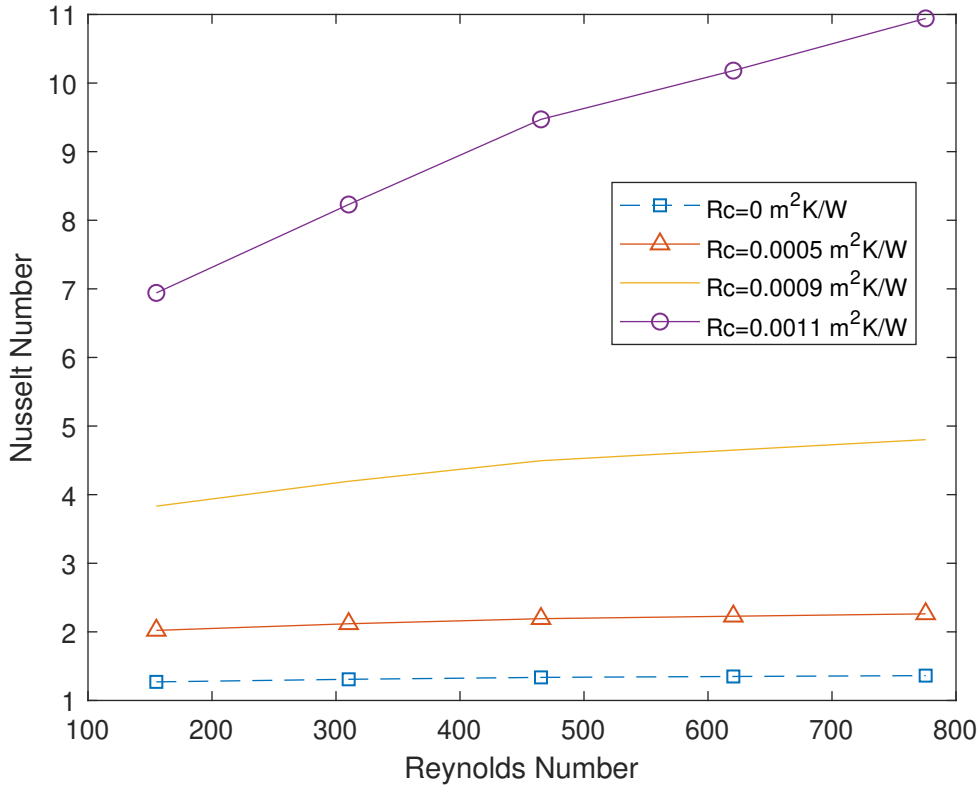

Figure 4.13: The change in the Nusselt number as the contact resistance input in the data analysis changes.

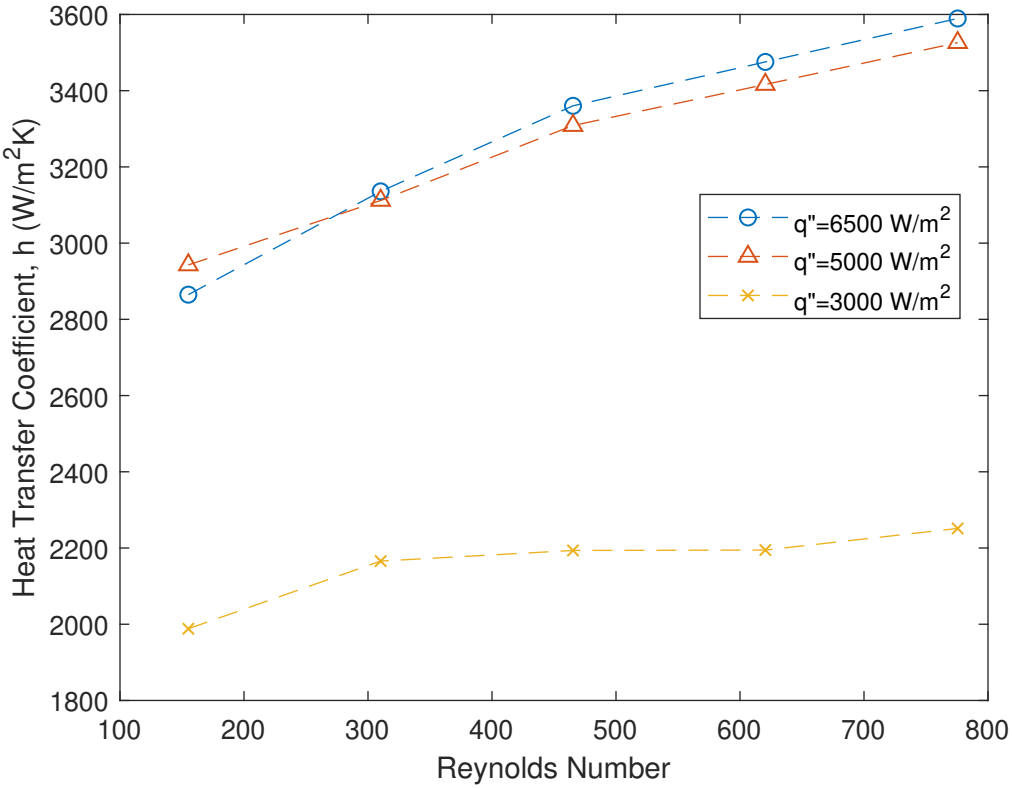

Figure 4.14: The change in the heat transfer coefficient as the heat flux changes at different Re number.

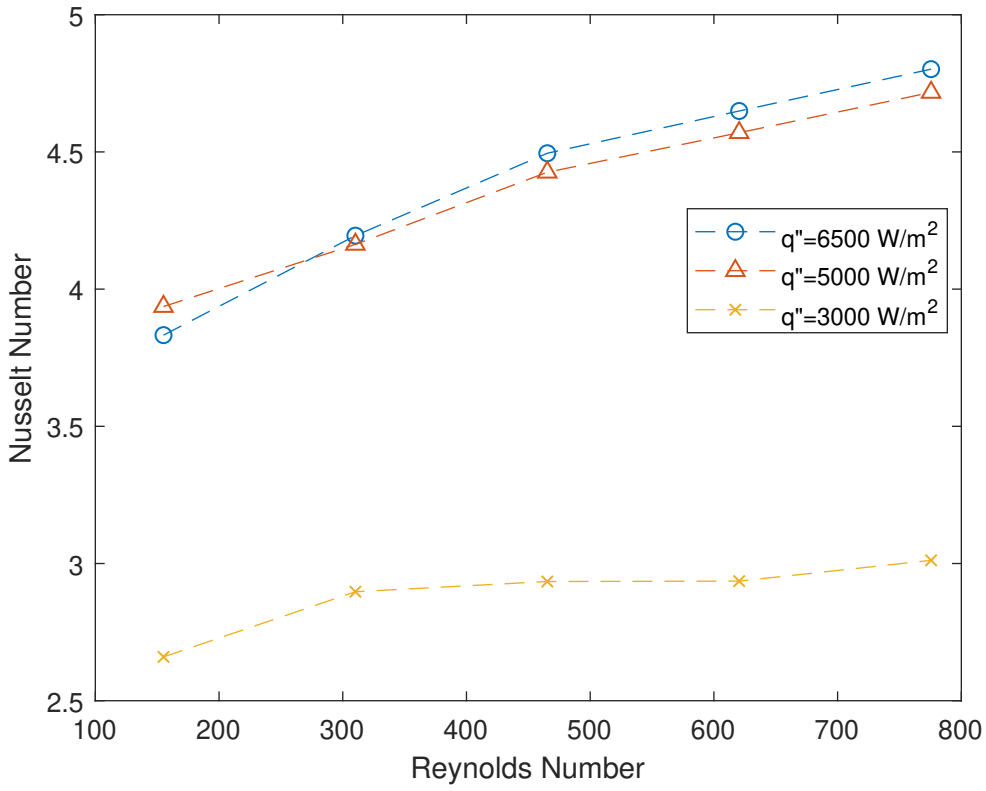

Figure 4.15: The change in the Nusselt as the heat flux changes at different Re number.

Chapter 5

Future Work

This experimental line of work has many directions and possibilities that can be examined further in the future. Several areas for future work are summarized below:

- **Material of the Heat Sink**. The material used in this experiment is stainless steel, which has a relatively low thermal conductivity of $16.2 W/m*K$. A material with higher thermal conductivity, like copper or aluminium, should be tested as those materials are more suitable for the application of electronics cooling. However, at the present time, these materials are somewhat more difficult for fabrication through additive manufacturing.

- **Design of the Heat Sink**. The straight channel design allows for a direct comparison with well-established correlations. However, it does not utilize the full power of additive manufacturing. In future studies, designs that incorporate more complex features to increase maximize heat transfer or decrease pressure drop should be developed and compared to the straight channel design.

- **Limits of Manufacturing Process**. In this study, the minichannel heat sink had a hydraulic diameter of 0.8 mm. Further experiments and a capability study should be done on the limits of the manufacturing process and the smallest possible feature that can be printed with different materials.

- **Study of Contact Resistance**. As can be seen from the results section, the contact

resistance plays a significant role in the heat transfer results. Additional methods for characterizing and controlling the contact resistance, should be performed in future studies. Additionally, in the experiments one could improve the wall temperature measurement by drilling holes inside the heat sink wall and inserting small thermocouples into the heat sink wall.

- **Study of the Effect of Roughness on the Flow**. The additive manufacturing process has an inherently high surface roughness and, as seen in the results, it can lead to an early transition to turbulence. This effect of the surface roughness should be carefully examined in future studies as it has large effects on the hydraulic, and possibly the thermal, performance of the minichannel heat sink.

Chapter 6

Conclusions

The thermal and hydraulic performance of a minichannel heat sink manufactured from stainless steel using binder jetting was characterized. The mini-channel heat sink, with a hydraulic diameter of 0.8mm, was manufactured to be used in an electronics cooling application. This work highlights the difficulty of manufacturing small features using fine powder materials, such as copper, and binder jetting. Even though the design does not utilize the full power of additive manufacturing, it allows for a direct comparison with well-established correlations. The results also establish a baseline set of results for further enhancements in the design of minichannel heat sinks. The tested minichannel heat sink was manufactured using stainless steel 316 L powder and using binder jetting manufacturing technique from ExOne.

The heat sink was experimentally tested with a single-phase operation over a range of Reynolds numbers (150-1250).The hydraulic results showed that an early transition to turbulence occurs at around Re=500. The high surface roughness and the small channel size led to this transition, which limits the range that the hydraulic performance can be predicted. A good agreement between the correlation and the results can be noticed before Re=500.

A mismatch between the experimental thermal results and the correlation has be noticed and requires further investigation on the reason. The effect of the contact resistance on the thermal results has been studied and are shown to be significant. Lastly, the recommended future work has been presented. The following lists summarises the findings and conclusions of this study:

1. The binder jetting additive manufacturing method can be used to fabricate a minichannel heat sink using Stainless Steel 316 L and with a hydraulic diameter of 0.8 mm for electronics cooling. The dimensions of the heat sink were chosen based on a survey of common CPU processor sizes, and the critical dimensions of the channels were based on the limits of the manufacturing machine. A capability study of the limits of the machine is recommended to investigate the smallest possible channel dimensions.

2. Challenges still rise when trying to fabricate small features using fine powder particles. In this study, an attempt to manufacture the heat sink using fine ($5\mu m$) copper powder has failed during the depowdering process. Because of the extremely small particle sizes, depowdering the channels has resulted in cracking of the samples. Further work can be done to investigate methods to use copper powder to manufacture minichannels.

3. The hydraulic performance of the straight minichannel heat sink was experimentally investigated for Reynolds numbers between 150-1250. The hydraulic results were compared to well-established correlation from the literature. The results showed a good agreement between the correlation and the experimental values up until Re=500. The experimental results start deviating from the correlation after Re=500, which signals that the flow has started transitioning to turbulence. This early transition can be attributed to the high surface roughness associated with the manufacturing process coupled with the small hydraulic diameter. The early transition to turbulence limits the range at which the performance can be predicted and it has to be considered in future designs of additively manufactured minichannels.

4. The Thermal performance of the heat sink was also experimentally investigated for Reynolds numbers between 150-800, where the temperatures and heat flux are measured, and the heat transfer coefficient is calculated. The thermal results are also compared to an established correlation. There is a mismatch between the correlation

and the experimental data that needs further investigating.

5. The effects of the contact resistance have been investigated and are shown to have significant effect on the thermal results due to uncertainty in the wall temperature measurement. The contact resistance could be the cause behind the mismatch between the correlation and the hydraulic results. Drilling holes inside the heat sinks an inserting thermocouples directly into the walls of the heat sink is one method that can reduce the effect of the contact resistance.

6. The study concludes with a future works section that examines some further directions that can be investigated in the future. Testing different materials and channel sizes are some of the next steps for this study.

Bibliography

[1] Tisha Dixit and Indranil Ghosh. Review of micro- and mini-channel heat sinks and heat exchangers for single phase fluids. *Renewable and Sustainable Energy Reviews*, 41:1298–1311, 2015.

[2] H. Ghaedamini, P. S. Lee, and C. J. Teo. Developing forced convection in converging–diverging microchannels. *International Journal of Heat and Mass Transfer*, 65:491–499, 2013.

[3] 2012.

[4] A. Dewan and P. Srivastava. A review of heat transfer enhancement through flow disruption in a microchannel. *Journal of Thermal Science*, 24(3):203–214, 2015.

[5] S. Krishnan, S. V. Garimella, G. M. Chrysler, and R. V. Mahajan. Towards'a thermal moore's law. *Ieee Transactions on Advanced Packaging*, 30(3):462–474, 2007.

[6] M. Rahimi, E. Karimi, M. Asadi, and P. Valeh-e Sheyda. Heat transfer augmentation in a hybrid microchannel solar cell. *International Communications in Heat and Mass Transfer*, 43:131–137, 2013.

[7] D. B. Tuckerman and R. F. W. Pease. High-performance heat sinking for vlsi. *IEEE Electron Device Letters*, 2(5):126–129, 1981.

[8] R. W. Keyes. Physical limits in digital electronics. *Proceedings of the IEEE*, 63(5):740–767, 1975.

[9] Satish Kandlikar and William Grande. Evolution of microchannel flow passages–thermohydraulic performance and fabrication technology. *Heat Transfer Engineering*, 24, 2003.

[10] Y. J. Lee, P. S. Lee, and S. K. Chou. Enhanced thermal transport in microchannel using oblique fins. *Journal of Heat Transfer*, 134(10), 2012.

[11] D. B. Tuckerman and R. F. W. Pease. High-performance heat sinking for vlsi. *IEEE Electron Device Letters*, 2(5):126–129, 1981.

[12] R.J. Phillips and Lincoln Laboratory. *Forced-convection, Liquid-cooled, Microchannel Heat Sinks*. Massachusetts Institute of Technology, Department of Mechanical Engineering, 1987.

[13] S. G. Kandlikar, H. R. Upadhye, and Ieee. *Extending the heat flux limit with enhanced microchannels in direct single-phase cooling of computer chips*, pages 8–15. Proceedings IEEE Semiconductor Thermal Measurement and Management Symposium. Ieee, New York, 2005.

[14] Himanshu Pokharna, Kuroda Masahiro, Eric DiStefano, Rajiv Mongia, Jim Barry, Chris Crowley, Weibo Chen, and Mike Izenson. Microchannel cooling in computing platforms: Performance needs and challenges in implementation. In *ASME 2004 2nd International Conference on Microchannels and Minichannels*, volume ASME 2nd International Conference on Microchannels and Minichannels, pages 109–118.

[15] T. A. Ameel, R. O. Warrington, R. S. Wegeng, and M. K. Drost. Miniaturization technologies applied to energy systems. *Energy Conversion and Management*, 38(10-13):969–982, 1997.

[16] M. Gad-el Hak. The mems handbook.

[17] N. T. Nguyen. Micromachined flow sensors - a review. *Flow Measurement and Instrumentation*, 8(1):7–16, 1997.

[18] A. R. Abramson and C. L. Tien. Recent developments in microscale thermophysical engineering. *Microscale Thermophysical Engineering*, 3(4):229–244, 1999.

[19] A. Datta, D. Sanyal, A. Agrawal, and A. K. Das. A review of liquid flow and heat transfer in microchannels with emphasis to electronic cooling. *Sadhana-Academy Proceedings in Engineering Sciences*, 44(12):32, 2019.

[20] T. Dixit and I. Ghosh. Review of micro- and mini-channel heat sinks and heat exchangers for single phase fluids. *Renewable Sustainable Energy Reviews*, 41:1298–1311, 2015.

[21] P. Gunnasegaran, H. A. Mohammed, N. H. Shuaib, and R. Saidur. The effect of geometrical parameters on heat transfer characteristics of microchannels heat sink with different shapes. *International Communications in Heat and Mass Transfer*, 37(8):1078–1086, 2010.

[22] G. L. Morini. Laminar-to-turbulent flow transition in microchannels. *Microscale Thermophysical Engineering*, 8(1):15–30, 2004.

[23] G. L. Morini. Single-phase convective heat transfer in microchannels: a review of experimental results. *International Journal of Thermal Sciences*, 43(7):631–651, 2004.

[24] Zhuo Li, Wen-Quan Tao, and Ya-Ling He. A numerical study of laminar convective heat transfer in microchannel with non-circular cross-section a preliminary version of this paper was presented at icmm05: Third international conference on microchannels and minichannels, held at university of toronto, june 13–15, 2005, organized by s.g. kandlikar and m. kawaji, cd-rom proceedings, isbn: 0-7918-3758-0, asme, new york. *International Journal of Thermal Sciences*, 45(12):1140–1148, 2006.

[25] Rajashankar Sadasivam, Raj M. Manglik, and Milind A. Jog. Fully developed forced convection through trapezoidal and hexagonal ducts. *International Journal of Heat and Mass Transfer*, 42(23):4321–4331, 1999.

[26] Sandip K. Saha, Amit Agrawal, and Yogesh Soni. Heat transfer characterization of rhombic microchannel for h1 and h2 boundary conditions. *International Journal of Thermal Sciences*, 111:223–233, 2017.

[27] Y. D. Hu, C. Werner, and D. Q. Li. Influence of three-dimensional roughness on pressure-driven flow through microchannels. *Journal of Fluids Engineering-Transactions of the Asme*, 125(5):871–879, 2003.

[28] A. S. Rawool, S. K. Mitra, and S. G. Kandlikar. Numerical simulation of flow through microchannels with designed roughness. *Microfluidics and Nanofluidics*, 2(3):215–221, 2006.

[29] W. Escher, T. Brunschwiler, N. Shalkevich, A. Shalkevich, T. Burgi, B. Michel, and D. Poulikakos. On the cooling of electronics with nanofluids. *Journal of Heat Transfer*, 133(5), 2011.

[30] Ahmed F. Al-Neama, Nikil Kapur, Jonathan Summers, and Harvey M. Thompson. An experimental and numerical investigation of the use of liquid flow in serpentine microchannels for microelectronics cooling. *Applied Thermal Engineering*, 116:709–723, 2017.

[31] Y. Sui, C. J. Teo, P. S. Lee, Y. T. Chew, and C. Shu. Fluid flow and heat transfer in wavy microchannels. *International Journal of Heat and Mass Transfer*, 53(13):2760–2772, 2010.

[32] Y. Sui, P. S. Lee, and C. J. Teo. An experimental study of flow friction and heat transfer

in wavy microchannels with rectangular cross section. *International Journal of Thermal Sciences*, 50(12):2473–2482, 2011.

[33] H. A. Mohammed, P. Gunnasegaran, and N. H. Shuaib. Numerical simulation of heat transfer enhancement in wavy microchannel heat sink. *International Communications in Heat and Mass Transfer*, 38(1):63–68, 2011.

[34] H. A. Mohammed, P. Gunnasegaran, and N. Shuaib. Influence of channel shape on the thermal and hydraulic performance of microchannel heat sink. *International Communications in Heat and Mass Transfer*, 38:474–480, 2011.

[35] M. Khoshvaght-Aliabadi, S. M. Hassani, S. H. Mazlowni, and M. Nekoei. Effects of nooks configuration on hydrothermal performance of zigzag channels for nanofluid-cooled microelectronic heat sink. *Microelectronics Reliability*, 79:153–165, 2017.

[36] V. S. Duryodhan, Abhimanyu Singh, S. G. Singh, and Amit Agrawal. Convective heat transfer in diverging and converging microchannels. *International Journal of Heat and Mass Transfer*, 80:424–438, 2015.

[37] M. K. D. Chakravarthii, D. Mutharasu, and S. Shanmugan. Experimental and numerical investigation of pressure drop and heat transfer coefficient in converging-diverging microchannel heat sink. *Heat and Mass Transfer*, 53(7):2265–2277, 2017.

[38] V. S. Duryodhan, S. G. Singh, and A. Agrawal. Liquid flow through converging microchannels and a comparison with diverging microchannels. *Journal of Micromechanics and Microengineering*, 24(12), 2014.

[39] K. Kumar, R. Kumar, and R. S. Bharj. Entropy generation analysis due to heat transfer and nanofluid flow through microchannels: a review. *International Journal of Exergy*, 31(1):49–86, 2020.

[40] A. Dewan and P. Srivastava. A review of heat transfer enhancement through flow disruption in a microchannel. *Journal of Thermal Science*, 24(3):203–214, 2015.

[41] X. J. Wei, Y. K. Joshi, and P. M. Ligrani. Numerical simulation of laminar flow and heat transfer inside a microchannel with one dimpled surface. *Journal of Electronic Packaging*, 129(1):63–70, 2006.

[42] Minghai Xu, Hui Lu, Liang Gong, John C. Chai, and Xinyue Duan. Parametric numerical study of the flow and heat transfer in microchannel with dimples. *International Communications in Heat and Mass Transfer*, 76:348–357, 2016.

[43] E. G. Colgan, B. Furman, A. Gaynes, W. Graham, N. LaBianca, J. H. Magerlein, R. J. Polastre, M. B. Rothwell, R. J. Bezama, R. Choudhary, K. Marston, H. Toy, J. Wakil, and J. Zitz. A practical implementation of silicon microchannel coolers for high power chips. In *Semiconductor Thermal Measurement and Management IEEE Twenty First Annual IEEE Symposium, 2005.*, pages 1–7.

[44] Y. H. Xie, Z. Y. Shen, D. Zhang, and J. B. Lan. Thermal performance of a water-cooled microchannel heat sink with grooves and obstacles. *Journal of Electronic Packaging*, 136(2), 2014.

[45] Hojatollah Gholami, M. Banaei, and A. Eskandari. Investigation of effect of triangular rib in heat transfer of finned rectangular microchannel with extended surfaces. *Life Science Journal*, 10:206–211, 2013.

[46] Guodong Xia, Lei Chai, Haiyan Wang, Ming Zheng Zhou, and Zhenzhen Cui. Optimum thermal design of microchannel heat sink with triangular reentrant cavities. *Applied Thermal Engineering - APPL THERM ENG*, 31:1208–1219, 2011.

[47] G. D. Xia, L. Chai, M. Z. Zhou, and H. Y. Wang. Effects of structural parameters

on fluid flow and heat transfer in a microchannel with aligned fan-shaped reentrant cavities. *International Journal of Thermal Sciences*, 50(3):411–419, 2011.

[48] G. D. Xia, Y. L. Zhai, and Z. Z. Cui. Numerical investigation of thermal enhancement in a micro heat sink with fan-shaped reentrant cavities and internal ribs. *Applied Thermal Engineering*, 58(1-2):52–60, 2013.

[49] Marc J Madou. *Fundamentals of microfabrication: the science of miniaturization*. CRC press, 2002.

[50] I. L. Collins, J. A. Weibel, L. Pan, and S. V. Garimella. Evaluation of additively manufactured microchannel heat sinks. *IEEE Transactions on Components, Packaging and Manufacturing Technology*, 9(3):446–457, 2019.

[51] C. K. Stimpson, J. C. Snyder, K. A. Thole, and D. Mongillo. Roughness effects on flow and heat transfer for additively manufactured channels. *Journal of Turbomachinery-Transactions of the Asme*, 138(5):10, 2016.

[52] C. K. Stimpson, J. C. Snyder, K. A. Thole, D. Mongillo, and Asme. *SCALING ROUGHNESS EFFECTS ON PRESSURE LOSS AND HEAT TRANSFER OF ADDITIVELY MANUFACTURED CHANNELS*. Proceedings of the Asme Turbo Expo: Turbine Technical Conference and Exposition, 2016, Vol 5b. Amer Soc Mechanical Engineers, New York, 2016.

[53] J. C. Snyder, C. K. Stimpson, K. A. Thole, and D. Mongillo. Build direction effects on additively manufactured channels. *Journal of Turbomachinery-Transactions of the Asme*, 138(5):8, 2016.

[54] Kathryn L. Kirsch and Karen A. Thole. Pressure loss and heat transfer performance

for additively and conventionally manufactured pin fin arrays. *International Journal of Heat and Mass Transfer*, 108:2502–2513, 2017.

[55] Kathryn Kirsch, Jacob Snyder, Curtis Stimpson, Karen Thole, and Dominic Mongillo. *Repeatability in Performance of Micro Cooling Geometries Manufactured with Laser Powder Bed Fusion*. 2017.

[56] M. A. Arie, A. H. Shooshtari, V. V. Rao, S. V. Dessiatoun, and M. M. Ohadi. Air-side heat transfer enhancement utilizing design optimization and an additive manufacturing technique. *Journal of Heat Transfer-Transactions of the Asme*, 139(3):12, 2017.

[57] M. A. Arie, A. H. Shooshtari, S. V. Dessiatoun, M. M. Ohadi, and Asme. *Performance Characterization of an Additively Manufactured Titanium (Ti64) Heat Exchanger for an Air-water Cooling Application*. Proceedings of the Asme Summer Heat Transfer Conference, 2016, Vol 2. Amer Soc Mechanical Engineers, New York, 2016.

[58] E. M. Dede, S. N. Joshi, and F. Zhou. Topology optimization, additive layer manufacturing, and experimental testing of an air-cooled heat sink. *Journal of Mechanical Design*, 137(11):9, 2015.

[59] Standard.

[60] Sharon L.N. Ford. Additive manufacturing technology: Potential implications for u.s. manufacturing competitiveness. *Economics of Innovation eJournal*, 2014.

[61] Christian Bergmann, Markus Lindner, Wen Zhang, Karolina Koczur, Armin Kirsten, Rainer Telle, and Horst Fischer. 3d printing of bone substitute implants using calcium phosphate and bioactive glasses. *Journal of the European Ceramic Society*, 30(12):2563–2567, 2010.

[62] Jooho Moon, Amador Caballero, Leszek Hozer, Yet-Ming Chiang, and Michael Cima. Fabrication of functionally graded reaction infiltrated sic–si composite by three-dimensional printing (3dp (tm)) process. *Materials Science and Engineering: A*, 298:110–119, 2001.

[63] Yun Bai and B. Williams Christopher. An exploration of binder jetting of copper. *Rapid Prototyping Journal*, 21(2):177–185, 2015.

[64] H. Miyanaji. Binder jetting additive manufacturing process fundamentals and the resultant influences on part quality.

[65] R.K. Shah, A.L. London, T.F. Irvine, and J.P. Hartnett. *Laminar Flow Forced Convection in Ducts: A Source Book for Compact Heat Exchanger Analytical Data*. Elsevier Science, 2014.

[66] Mark E. Steinke and Satish G. Kandlikar. Single-phase liquid friction factors in microchannels. *International Journal of Thermal Sciences*, 45(11):1073 – 1083, 2006.

[67] P. S. Lee and S. V. Garimella. Thermally developing flow and heat transfer in rectangular microchannels of different aspect ratios. *International Journal of Heat and Mass Transfer*, 49(17-18):3060–3067, 2006.

[68] R. Shah and A. London. Laminar flow forced convection in ducts: A source book for compact heat exchanger analytical data. 2014.

[69] X. F. Peng and G. P. Peterson. Convective heat transfer and flow friction for water flow in microchannel structures. *International Journal of Heat and Mass Transfer*, 39(12):2599–2608, 1996.

[70] Hamidreza Rastan, Amir Abdi, Monika Ignatowicz, Bejan Hamawandi, Poh Seng Lee, and Björn Palm. Heat transfer investigation of an additively manufactured minichan-

nel heat exchanger. In *ASME 2019 17th International Conference on Nanochannels, Microchannels, and Minichannels*, volume ASME 2019 17th International Conference on Nanochannels, Microchannels, and Minichannels, V001T01A001.